

Unsteady flows modeling and computation

Franck Nicoud *

University Montpellier II and I3M-CNRS UMR 5149, France

franck.nicoud@univ-montp2.fr

November 19, 2007

Contents

1	Introduction	3
2	The governing equations	5
3	Large-Eddy Simulations	7
3.1	The LES Concept	7
3.2	The Governing Equations	8
3.3	Models for ν_{SGS}	10
3.3.1	Static models	10
3.3.2	Transport model	12
3.3.3	Dynamic procedure	13
4	Boundary Conditions	17
4.1	General formalism	18
4.1.1	Full residual approach	22
4.1.2	Normal approach	22
4.1.3	Non-reflecting boundary conditions	22
4.1.4	About the Riemann invariants	24
4.2	Comparison of non-reflecting BC	24
4.2.1	One-dimensional cases	25
4.2.2	Two-dimensional shear-layer	26
4.2.3	Two-dimensional vortex	28
4.3	More about BC treatments	32
4.3.1	Linear relaxation	32
4.3.2	Approximate boundary conditions	35
4.3.3	Integral boundary conditions	39

*Some parts of this course have been adapted from the Handbook of the AVBP code developed at CERFACS (<http://www.cerfacs.fr/cfd/software.php>). The author would like to acknowledge all the contributors to this handbook, and especially T. Poinso, L. Gicquel, G. Staffelbach, T. Schönfeld, G. Lartigue, O. Colin

4.3.4	Advanced non-reflecting conditions	40
5	Numerical issues	43
5.1	Effective wave number	43
5.2	Handling stability issues	47
5.2.1	Kinetic energy conservation	48
5.2.2	Artificial viscosity	51
A	Governing equations for a multi-species, reacting gaseous mixture	61
A.1	Thermodynamical variables	62
A.2	The equation of state	62
A.3	Conservation of Mass: Species diffusion flux	63
A.4	Viscous stress tensor	64
A.5	Heat flux vector	64
A.6	Transport coefficients	64

1 Introduction

Over the last decades, algorithmic improvements and increase of computational power have led to solvers with higher levels of accuracy. A major subject for industrial computation has been, and still is, steady state flow. It is important to converge rapidly to steady state, and it has been recognized that dissipative schemes help, but detriment the accuracy.

In some cases, the average quantities are not relevant to the flow physics. Consider for example the time evolution of temperature T at a position where a flame is moving back and forth. To the first order, T is alternatively equal to the burnt gas temperature, $T_b = 1500$ K say, and to the fresh gas temperature, $T_u = 300$ K say. A perfect assessment of the average temperature would lead to $(T_b + T_u)/2$, viz. 900 K in the example. Clearly enough this value is not relevant to the thermodynamic state of the gas and only an unsteady computation could really provide useful information. More generally, accurate computation of unsteady compressible flow is needed in aero-acoustics, self-sustained instabilities and combustion instabilities, combustion noise, flame dynamics description, etc ...

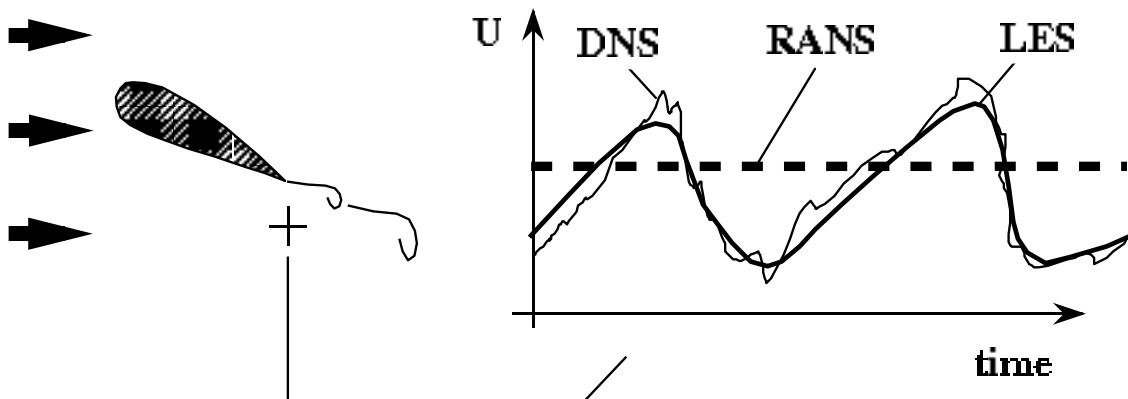


Figure 1: Principle of the DNS, RANS and LES approaches. Typical time evolutions of velocity that these three methods would provide downstream of a trailing edge at large angle of attack.

Typical approaches are:

- Direct Numerical Simulation (DNS): the Navier-Stokes equations are solved without additional modeling. Due to the scale separation in turbulent flows, this approach would require a huge amount of grid points for practical applications. Since only averaged quantities can be compared or used for modeling purposes, a statistical treatment of the 3D unsteady solution is required after the simulation has been completed. The DNS approach provides all the flow details (see figure 1) but it is only suitable to perform fundamental studies of academic configurations with moderate Reynolds number. See Moin and Mahesh (1998) for a recent review,
- Reynolds-Averaged Navier-Stokes equations (RANS): a statistical treatment is applied to the Navier-Stokes equations which are then solved to provide average quantities (see figure 1) directly. In doing so, the small scales are not present in the

equations and less demand is put on the numerical method and mesh requirement. This is the method mostly used in modern design chain to reduce the number of experimental testing. The price to pay is the need to model the correlations which appear when averaging the non-linear terms of the basic equations. This task proves extremely difficult and it is nowadays accepted that no general turbulence model exists, limiting the generality and the predictive potential of the RANS approach,

- Large Eddy Simulation (LES): the Navier-Stokes equations are low-pass filtered before the numerical solution is sought. In doing so, only the small scales must be modeled, the largest ones being computed directly (see figure 1). This approach can be thought as an intermediate between the DNS and the RANS approaches. It put more demand on the numerics than the RANS approach does, but requires less modeling effort because the small scales are more universal in nature. It has already been used quite often in place of DNS to address fundamental issues in simple configurations (Mendez and Nicoud, 2008); it also has the greatest potential for practical use in the industry (Schmitt et al., 2007).

The objective of this course is to address some of the issues which arise when designing tools for unsteady flows. The basic governing equations for the compressible flow of an homogeneous gas are recall in section §2 and some details about the Large Eddy Simulation approach are given in section §3. The theory of characteristic-based boundary conditions is given in section §4.1 while the importance of their numerical implementation is illustrated in section §4.2. The last part is more devoted to numerical issues: the spectral analysis of numerical schemes is described in section §5.1 and techniques for the stabilization of computations based on low-dissipative schemes are discussed in section §5.2 for both the incompressible and the compressible flow equations.

2 The governing equations

Throughout this document, the index notation is adopted for the description of the governing equations. Summation rule is henceforth implied over repeated indices (Einstein's rule of summation). For sake of simplicity, only the simple case of an homogeneous gas is considered in the main text. The governing equations for the case of a chemically reacting multi-species mixture are more relevant to combustion instabilities; they are given in annex for completeness.

The set of conservation equation describing the evolution of a compressible flow reads:

$$\frac{\partial \rho u_i}{\partial t} + \frac{\partial}{\partial x_j}(\rho u_i u_j) = - \frac{\partial}{\partial x_j}[P \delta_{ij} - \tau_{ij}], \quad (1)$$

$$\frac{\partial \rho E}{\partial t} + \frac{\partial}{\partial x_j}(\rho E u_j) = - \frac{\partial}{\partial x_j}[u_i (P \delta_{ij} - \tau_{ij}) + q_j], \quad (2)$$

$$\frac{\partial \rho}{\partial t} + \frac{\partial}{\partial x_j}(\rho u_j) = 0. \quad (3)$$

Equations 1-3 correspond to the conservation of momentum, total energy and mass respectively, and ρ , u_i and E denote density, the velocity vector, the total energy per unit mass.

It is usual to decompose the flux tensor into an inviscid and a viscous component. The inviscid part reads:

$$\begin{pmatrix} \rho u_i u_j + P \delta_{ij} \\ (\rho E + P \delta_{ij}) u_j \\ \rho u_j \end{pmatrix} \quad (4)$$

where the hydrostatic pressure P is given by the equation of state for a perfect gas, viz. $P = \rho r T$, where r is the gas constant of the mixture, $r = \frac{R}{W}$, W being the mean molecular weight and $R = 8.3143$ J/mol.K the universal gas constant. The adiabatic exponent is given by $\gamma = C_p/C_v$.

The components of the viscous flux tensor take the form:

$$\begin{pmatrix} -\tau_{ij} \\ -(u_i \tau_{ij}) + q_j \\ 0 \end{pmatrix} \quad (5)$$

The stress tensor τ_{ij} is given by the following relations:

$$\tau_{ij} = 2\mu(S_{ij} - \frac{1}{3}\delta_{ij}S_{ll}), \quad (6)$$

and

$$S_{ij} = \frac{1}{2}\left(\frac{\partial u_j}{\partial x_i} + \frac{\partial u_i}{\partial x_j}\right), \quad (7)$$

Eq. 6 may also be written:

$$\begin{aligned} \tau_{xx} &= \frac{2\mu}{3}\left(2\frac{\partial u}{\partial x} - \frac{\partial v}{\partial y} - \frac{\partial w}{\partial z}\right), & \tau_{xy} &= \mu\left(\frac{\partial u}{\partial y} + \frac{\partial v}{\partial x}\right) \\ \tau_{yy} &= \frac{2\mu}{3}\left(2\frac{\partial v}{\partial y} - \frac{\partial u}{\partial x} - \frac{\partial w}{\partial z}\right), & \tau_{xz} &= \mu\left(\frac{\partial u}{\partial z} + \frac{\partial w}{\partial x}\right) \\ \tau_{zz} &= \frac{2\mu}{3}\left(2\frac{\partial z}{\partial z} - \frac{\partial u}{\partial x} - \frac{\partial v}{\partial y}\right), & \tau_{yz} &= \mu\left(\frac{\partial v}{\partial z} + \frac{\partial w}{\partial y}\right) \end{aligned} \quad (8)$$

where μ is the shear viscosity.

The heat flux is given by

$$q_i = -\lambda \frac{\partial T}{\partial x_i}, \quad (9)$$

where λ is the heat conduction coefficient of the gas.

The molecular viscosity μ is often assumed to be given by the classical Sutherland law:

$$\mu = c_1 \frac{T^{3/2}}{T + c_2} \frac{T_{ref} + c_2}{T_{ref}^{3/2}} \quad (10)$$

where c_1 and c_2 must be determined so as to fit the real viscosity of the mixture. For air at $T_{ref} = 273$ K, $c_1 = 1.71 \times 10^{-5}$ kg/m.s and $c_2 = 110.4$ K (see White (1999)). A second law is sometimes preferred, called Power law:

$$\mu = c_1 \left(\frac{T}{T_{ref}} \right)^b \quad (11)$$

with b typically ranging between 0.5 and 1.0. For example $b = 0.76$ for air. The heat conduction coefficient can be computed by introducing the molecular Prandtl number :

$$\lambda = \frac{\mu C_p}{P_r} \quad (12)$$

Note that P_r is usually supposed as constant in time and space.

3 Large-Eddy Simulations

3.1 The LES Concept

In comparison to the more classical Reynolds Averaged Navier-Stokes (RANS) methodologies, Large Eddy Simulation (LES) (Sagaut, 1998; Pope, 2002) is nowadays recognized as the approach with the highest potential as far as unsteady flows are concerned. Although conceptually very different, these two approaches aim at providing new systems of governing equations to mimic the characteristics of turbulent flows.

The new governing equations are obtained by introducing operators to be applied to the set of compressible Navier-Stokes equations. Unclosed terms arise from these manipulations and models need to be supplied for the problem to be solved. The major differences between RANS and LES come from the operator employed in the derivation. In RANS the operation consists of a temporal or ensemble average over a set of realizations of the studied flow (Pope, 2002; Chassaing, 2000). The unclosed terms are representative of the physics taking place over the entire range of frequencies present in the ensemble of realizations under consideration. In LES, the operator is a spatially localized time independent filter of given size, Δ , to be applied to a single realization of the studied flow. Resulting from this spatial filtering is a separation between the large (greater than the filter size) and small (smaller than the filter size) scales. In LES, the unclosed terms are representative of the physics associated with the smallest structures (with highest frequencies) present in the flow. Figure 2 illustrates the conceptual differences between (a) RANS and (b) LES when applied to a homogeneous isotropic turbulent field.

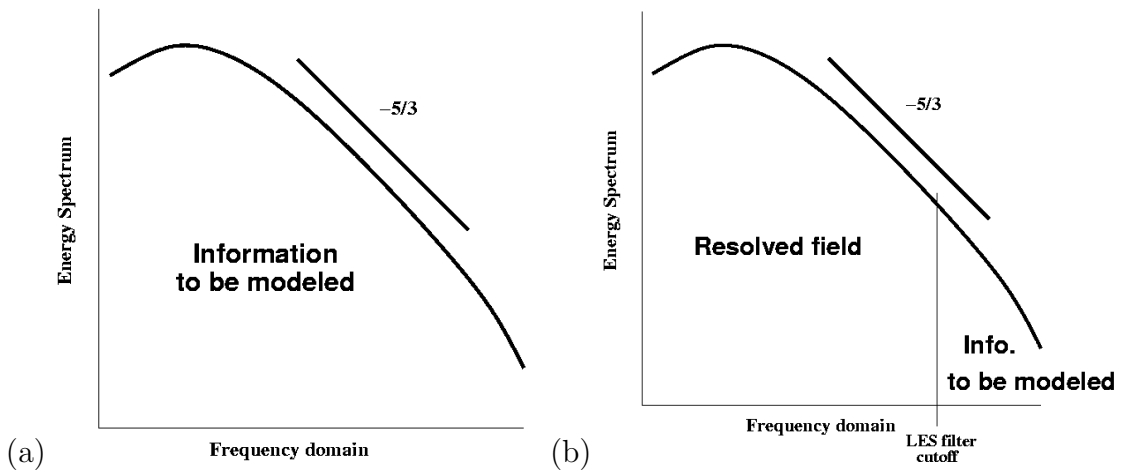


Figure 2: Conceptual representation of (a) RANS and (b) LES applied to a homogeneous isotropic turbulent field.

Due to the filtering approach, LES allows a dynamic representation of the large scale motions whose contributions are critical in complex geometries. The LES predictions of complex turbulent flows are henceforth closer to the physics since large scale phenomena such as large vortex shedding and acoustic waves are embedded in the set of governing equations.

For the reasons presented above, LES has a clear potential in predicting turbulent

flows encountered in industrial applications. Such possibilities are however restricted by the hypothesis introduced while constructing LES models.

3.2 The Governing Equations

The filtered quantity \bar{f} is resolved in the numerical simulation whereas $f' = f - \bar{f}$ is the subgrid scale part due to the unresolved flow motion. For variable density ρ , a mass-weighted Favre filtering is introduced such as:

$$\bar{\rho} \tilde{f} = \overline{\rho f} \quad (13)$$

The balance equations for large eddy simulations are obtained by filtering the instantaneous balance equations 1, 2 and 3:

$$\frac{\partial \bar{\rho} \tilde{u}_i}{\partial t} + \frac{\partial}{\partial x_j} (\bar{\rho} \tilde{u}_i \tilde{u}_j) = - \frac{\partial}{\partial x_j} [\bar{P} \delta_{ij} - \bar{\tau}_{ij} - \bar{\tau}_{ij}^t], \quad (14)$$

$$\frac{\partial \bar{\rho} \tilde{E}}{\partial t} + \frac{\partial}{\partial x_j} (\bar{\rho} \tilde{E} \tilde{u}_j) = - \frac{\partial}{\partial x_j} [\overline{u_i (P \delta_{ij} - \tau_{ij})} + \bar{q}_j + \bar{q}_j^t], \quad (15)$$

$$\frac{\partial \bar{\rho}}{\partial t} + \frac{\partial}{\partial x_j} (\bar{\rho} \tilde{u}_j) = 0, \quad (16)$$

where a repeated index implies summation over this index (Einstein's rule of summation). The cut-off scale usually corresponds to the mesh size (implicit filtering); moreover, one often assumes that the filter operator and the partial derivative commute.

In Eqs. 14, 15 and 16, the flux tensor can be divided in three parts: the inviscid part, the viscous part and the subgrid scale turbulent part.

The three spatial components of the inviscid flux tensor are the same as in DNS but based on the filtered quantities:

$$\begin{pmatrix} \bar{\rho} \tilde{u}_i \tilde{u}_j + \bar{P} \delta_{ij} \\ \bar{\rho} \tilde{E} \tilde{u}_j + \bar{P} u_j \delta_{ij} \\ \bar{\rho}_k \tilde{u}_j \end{pmatrix} \quad (17)$$

The components of the viscous flux tensor take the form:

$$\begin{pmatrix} -\bar{\tau}_{ij} \\ -(\bar{u}_i \bar{\tau}_{ij}) + \bar{q}_j \\ 0 \end{pmatrix} \quad (18)$$

Filtering the balance equations leads to unclosed quantities, which need to be modeled. The components of the turbulent subgrid scale flux take the form:

$$\begin{pmatrix} -\bar{\tau}_{ij}^t \\ \bar{q}_j^t \\ 0 \end{pmatrix} \quad (19)$$

The filtered diffusion terms are approximated in the following way :

$$\begin{aligned}\overline{\tau_{ij}} &= \overline{2\mu(S_{ij} - \frac{1}{3}\delta_{ij}S_u)}, \\ &\approx 2\overline{\mu}(\tilde{S}_{ij} - \frac{1}{3}\delta_{ij}\tilde{S}_u),\end{aligned}\quad (20)$$

and

$$\tilde{S}_{ij} = \frac{1}{2}\left(\frac{\partial\tilde{u}_j}{\partial x_i} + \frac{\partial\tilde{u}_i}{\partial x_j}\right),\quad (21)$$

In full, equation 20 may also be written:

$$\begin{aligned}\overline{\tau_{xx}} &\approx \frac{2\overline{\mu}}{3}\left(2\frac{\partial u}{\partial x} - \frac{\partial v}{\partial y} - \frac{\partial w}{\partial z}\right), & \overline{\tau_{xy}} &\approx \overline{\mu}\left(\frac{\partial u}{\partial y} + \frac{\partial v}{\partial x}\right) \\ \overline{\tau_{yy}} &\approx \frac{2\overline{\mu}}{3}\left(2\frac{\partial v}{\partial y} - \frac{\partial u}{\partial x} - \frac{\partial w}{\partial z}\right), & \overline{\tau_{xz}} &\approx \overline{\mu}\left(\frac{\partial u}{\partial z} + \frac{\partial w}{\partial x}\right) \\ \overline{\tau_{zz}} &\approx \frac{2\overline{\mu}}{3}\left(2\frac{\partial w}{\partial z} - \frac{\partial u}{\partial x} - \frac{\partial v}{\partial y}\right), & \overline{\tau_{yz}} &\approx \overline{\mu}\left(\frac{\partial v}{\partial z} + \frac{\partial w}{\partial y}\right)\end{aligned}\quad (22)$$

Regarding the filtered heat flux, one may write:

$$\overline{q_i} = -\overline{\lambda}\frac{\partial T}{\partial x_i} \approx -\overline{\lambda}\frac{\partial\tilde{T}}{\partial x_i}\quad (23)$$

These forms assume that the spatial variations of molecular diffusion fluxes are negligible and can be modeled through simple gradient assumptions.

The filtered compressible Navier-Stokes equations exhibit sub-grid scale (SGS) tensors and vectors describing the interaction between the non-resolved and resolved motions. The influence of the SGS on the resolved motion must be taken into account by a SGS model. At this stage, it is common use to rely on the SGS eddy-viscosity concept (Boussinesq assumption) to model the different contributions:

- the Reynolds tensor is :

$$\overline{\tau_{ij}^t} = -\overline{\rho}(\overline{u_i u_j} - \tilde{u}_i \tilde{u}_j) \approx 2\overline{\rho}\nu_{\text{SGS}}(\tilde{S}_{ij} - \frac{1}{3}\delta_{ij}\tilde{S}_u),\quad (24)$$

where the SGS eddy-viscosity ν_{SGS} will be modelled in section § 3.3.

- the subgrid scale heat flux vector is:

$$\overline{q_i^t} = \overline{\rho}(\overline{u_i E} - \tilde{u}_i \tilde{E}) \approx -\lambda_{\text{SGS}}\frac{\partial\tilde{T}}{\partial x_i},\quad (25)$$

with

$$\lambda_{\text{SGS}} = \frac{\rho\nu_{\text{SGS}}\overline{C_p}}{P_r^t}.\quad (26)$$

The turbulent Prandtl number is usually fixed in the range 0.5-0.9.

3.3 Models for ν_{SGS}

3.3.1 Static models

The first SGS model was proposed by Smagorinsky (1963) and has been heavily tested for multiple flow configurations in the last decades. In this model, the eddy-viscosity is assumed to be proportional to the subgrid characteristic length scale Δ and to a characteristic turbulent velocity taken as the local strain rate $|\overline{S}|$:

$$\nu_{\text{SGS}} = (C_s \Delta)^2 |\overline{S}|, \quad |\overline{S}| = \sqrt{2\overline{S}_{ij}\overline{S}_{ij}}. \quad (27)$$

Following Lilly (1992), the constant C_s may be obtained by assuming that the cut-off wave number $k_c = \pi/\Delta$ lies within a $k^{-5/3}$ Kolmogorov cascade for the energy spectrum $E(k) = C_K \epsilon^{2/3} k^{-5/3}$ and requiring that the ensemble-averaged subgrid dissipation is identical to ϵ . An approximate value for the constant is then:

$$C_s = \frac{1}{\pi} \left(\frac{3C_K}{2} \right)^{-3/4}.$$

For a Kolmogorov constant of $C_K \simeq 1.4$, this yields $C_s \simeq 0.18$. However, this constant value often leads to a significant over-estimation of the SGS dissipation and ad hoc procedure must be used in order to handle wall bounded flows.

Note that the choice of the local strain rate to define the velocity scale at the cut-off is quite arbitrary. If one considers that the velocity gradient tensor is a good candidate to describe the turbulent fluctuations, other invariants based on this tensor could be used for defining the velocity scale needed for the eddy-viscosity ν_{SGS} . The aim of this latter quantity is to mimic the energy transfer from the resolved scales to the subgrid ones through the subgrid dissipation (which is proportional to ν_{SGS}). Thus by defining the eddy-viscosity from the local strain rate, one relates the subgrid dissipation to the strain rate of the smallest resolved scales of motion. This choice is not in agreement with the results from Wray and Hunt (1989) on the kinematic and dynamic properties of the turbulent structures. From direct numerical simulations of isotropic turbulence, these authors have shown that energy is concentrated in the streams and energy dissipation in eddies and convergence zones. Clearly the classical Smagorinsky formulation does not account for the contribution of the former which are regions where vorticity dominates irrotational strain. On the other hand the dominant deformation in convergence zones is irrotational strain so that the strain rate could be a good measure of their dissipative activity. Thus a better subgrid scale model should be based on both $|\overline{S}|$ and the rotational rate. This requirement is met by the structure function model Metais and Lesieur (1992) which reads:

$$\nu_{\text{SGS}} = \beta C_K^{-3/2} \Delta \sqrt{\overline{F}_2}, \quad (28)$$

where \overline{F}_2 is the second order velocity structure function of the filtered field:

$$\overline{F}_2(\vec{x}, \Delta) = \langle ||\overline{\vec{u}}(\vec{x}, t) - \overline{\vec{u}}(\vec{x} + \vec{r}, t)||^2 \rangle_{||\vec{r}||=\Delta},$$

and β is a constant which can be fixed from energetic considerations. Very good results have been obtained with this model for isotropic homogeneous turbulence Lesieur

and Métais (1996). Other formulations have been proposed to assess the subgrid scale stress, based on the local strain and rotation rate tensors and products of them Lund and Novikov (1992).

An important point in LES is the behavior of the eddy-viscosity near solid walls. By construction, the Smagorinsky model gives a non-zero value of ν_{SGS} as soon as a velocity gradient exists. Near a wall, however, all turbulent fluctuations are damped so that ν_{SGS} should be zero. This is the reason why the Van Driest Van Driest (1956) exponential damping function $1 - \exp(-y^+/A^+)$ with $A^+ = 25$, was used widely in early LES studies. This standard modification improves the results dramatically and is very easy to implement for simple geometries. However, it is an *ad hoc* modification based on the distance to the wall. This is difficult to implement in the general case for complex geometries. It also requires the use of a smaller value for the Smagorinsky constant ($C_s = 0.1$) in order to sustain turbulence in a channel flow Moin and Kim (1982). Note also that depending on the damping function used it may not produce the proper near-wall scaling for the eddy-viscosity. The above-mentioned Van Driest damping produces $\nu_{\text{SGS}} = O(y^2)$ instead of $O(y^3)$. Neither is the classical structure function model well-suited for wall bounded flows. Indeed, the \overline{F}_2 function is of order $O(1)$ near a wall when computed as a local statistical average of square velocity differences between the current position and the six closest surrounding points on the (structured) computational grid. A possible remedy for this is to compute \overline{F}_2 by using only the four closest points parallel to a given plane. If the plane is parallel to the wall, \overline{F}_2 is of order $O(y)$ and better results are obtained in a boundary layer Comte et al. (1994); Ducros et al. (1996). Another way to produce zero eddy-viscosity at the wall is to modify the constant of the model (C_s for the Smagorinsky model) in such a way as to enforce $C_s \simeq 0$ when turbulence activity is reduced. This is done dynamically by the procedure proposed by Germano et al. (1991), in which the variable $C = C_s^2$ appears in five independent equations. More details about the dynamic procedure are provided in section §3.3.3.

All the above discussed models may be written in the generic form:

$$\nu_{\text{SGS}} = C_m \Delta^2 \overline{OP}(\vec{x}, t), \quad (29)$$

where C_m is the constant of the model, Δ is the subgrid characteristic length scale (in practice the size of the mesh) and \overline{OP} is an operator of space and time, homogeneous to a frequency, and defined from the resolved fields. An operator meeting the following properties would be a good candidate for SGS modeling purposes:

- it is invariant to any coordinate translation or rotation,
- it can be easily assessed on any kind of computational grid,
- it is a function of both the strain and the rotation rates, in agreement with recent findings concerning the contribution of the turbulent structures to the global dissipation,
- it goes naturally to zero at the wall so that neither damping function nor dynamic procedure are needed to reproduce the effect of the no-slip condition.

The WALE (Wall-Adapting Local Eddy-viscosity) model meets all the above requirements (Nicoud and Ducros, 1999). It reads:

$$s_{ij}^d = \frac{1}{2} (\tilde{g}_{ij}^2 + \tilde{g}_{ji}^2) - \frac{1}{3} \tilde{g}_{kk}^2 \delta_{ij}, \quad (30)$$

$$\nu_{\text{SGS}} = (C_w \Delta)^2 \frac{(s_{ij}^d s_{ij}^d)^{3/2}}{(\tilde{S}_{ij} \tilde{S}_{ij})^{5/2} + (s_{ij}^d s_{ij}^d)^{5/4}}, \quad (31)$$

where Δ denotes the filter characteristic length (cube-root of the cell volume), $C_w = 0.5$ is the model constant and \tilde{g}_{ij} denotes the resolved velocity gradient. This model is based on a tensor invariant and reproduces the proper scaling at the wall ($\nu_{\text{SGS}} = O(y^3)$). It is also well-suited for LES in complex geometries with structured or unstructured methods because no explicit filtering is needed and only local information is required to build the eddy-viscosity. Finally, it is sensitive to both the strain and the rotation rate of the small turbulent structures.

Note that C_m is considered here as a true constant, assessed from the canonic case of isotropic homogeneous turbulence. A potential improvement of the WALE model could be to use the dynamic procedure (see section §3.3.3) to compute this constant. It seems that this option has never been investigated so far although no major issue are expected related to the writing of the dynamic WALE model.

3.3.2 Transport model

A drawback of the above models is that they directly relate the level of turbulent viscosity to the local instantaneous resolved velocity gradients. Thus they cannot account for cases where local levels of sub-grid scale energy are high in regions of low resolved gradients, because the kinetic energy has been convected from regions with high sub-grid turbulence. To overcome this difficulty, one possibility is to assume that the SGS viscosity is deduced from the transported sub-grid scale turbulent kinetic energy k_{sgs} .

$$\nu_{\text{SGS}} = C_k \Delta k_{\text{sgs}}^{1/2} \quad (32)$$

where C_k is a model constant, Δ denotes the filter characteristic length (cube-root of the cell volume) and k_{sgs} is the subgrid-scale turbulent kinetic energy defined as:

$$k_{\text{sgs}} = \frac{1}{2} (\widetilde{u_i u_i} - \tilde{u}_i \tilde{u}_i) \quad (33)$$

The filtered transport equation for k_{sgs} reads:

$$\frac{\partial \bar{\rho} k_{\text{sgs}}}{\partial t} + \frac{\partial \bar{\rho} k_{\text{sgs}} \tilde{u}_j}{\partial x_j} = \frac{\partial}{\partial x_j} \left(\mu_t \frac{\partial k_{\text{sgs}}}{\partial x_j} \right) + \left(2\mu_t \tilde{S}_{ij} - \frac{2}{3} \bar{\rho} k_{\text{sgs}} \delta_{ij} \right) \frac{\partial \tilde{u}_i}{\partial x_j} - \bar{\rho} C_\epsilon \frac{k_{\text{sgs}}^{3/2}}{\Delta} \quad (34)$$

where the terms on the left-hand side represent the turbulent diffusion of k_{sgs} , its production and its dissipation.

The model constants C_K and C_ϵ can be shown to depend as follows from the standard Smagorinsky constant C_S :

$$C_k = \pi^{1/3} \left(\frac{2}{3 C_K} \right)^{1/2} (C_S)^{4/3}, \quad C_\epsilon = \pi \left(\frac{2}{3 C_K} \right)^{3/2} \quad (35)$$

yielding the following values for the standard values of $C_S = 0,18$ for a Homogeneous Isotropic Turbulence (HIT) without shear and $C_S = 0,1$ for a pure shear layer:

C_S	C_ϵ	C_k
0,18	1,03	0,10
0,10	1,03	0,05

The drawback of the approach is the necessity to solve one more transport equation.

3.3.3 Dynamic procedure

Most of the SGS models used in practical simulation rely on the so-called Boussinesq approximation and thus the key point in the SGS modeling is to devise an appropriate expression of the SGS eddy-viscosity. As mentioned earlier, and from a simple dimensional argument, such model for ν_{SGS} should read (see equation 29):

$$\nu_{\text{SGS}} = C_m \Delta^2 \overline{OP}(\vec{x}, t), \quad (36)$$

where C_m is the constant, Δ is the subgrid characteristic length scale (in practice the size of the local cell in the mesh) and \overline{OP} is an operator of space and time, homogeneous to a frequency, and defined from the resolved fields. If one accepts that the size of the local cell is the proper SGS characteristic length scale, there are only two ways of improving the model for ν_{SGS} : either improve the constant value C_m , or improve the frequency operator \overline{OP} ; the latter option has been discussed in section §3.3.1. This is the purpose of the dynamic procedure to provide the best possible value for C_m .

The dynamic procedure is rather general but it will be presented thereafter for the Smagorinsky model only, equation 27. The key point of this procedure is the so-called Germano identity which was discovered in the 90's (Germano et al., 1991). Recall that if a spatial filtering operation is applied to the flow motion equations, a SGS contribution appears which must be modeled (see equation 24). For sake of simplicity, let us consider here the case of an incompressible fluid. If the spatial filter $\overline{\cdot}$ (characteristic length Δ) is applied to the momentum equation:

$$\frac{\partial u_i}{\partial t} + \frac{\partial}{\partial x_j} (u_i u_j) = -\frac{1}{\rho} \frac{\partial}{\partial x_j} [P \delta_{ij} - \tau_{ij}], \quad (37)$$

the following LES equation is obtained (assuming no filter-derivative commutative error):

$$\frac{\partial \overline{u}_i}{\partial t} + \frac{\partial}{\partial x_j} (\overline{u}_i \overline{u}_j) = -\frac{1}{\rho} \frac{\partial}{\partial x_j} [\overline{P} \delta_{ij} - \overline{\tau}_{ij} - \tau_{ij}^{sgs}], \quad (38)$$

where τ_{ij}^{sgs} is the SGS stress tensor defined as:

$$\tau_{ij}^{sgs} = -\rho (\overline{u}_i \overline{u}_j - \overline{u}_i \overline{u}_j) \quad (39)$$

Let us define a second spatial filtering, noted $\widehat{\cdot}$ (characteristic length $\widehat{\Delta}$) and let us apply it to equation 38. This results in the following double filtered momentum equation:

$$\frac{\partial \widehat{\overline{u}}_i}{\partial t} + \frac{\partial}{\partial x_j} (\widehat{\overline{u}}_i \widehat{\overline{u}}_j) = -\frac{1}{\rho} \frac{\partial}{\partial x_j} [\widehat{\overline{P}} \delta_{ij} - \widehat{\overline{\tau}}_{ij} - \widehat{\tau}_{ij}^{sgs}], \quad (40)$$

where $\widehat{\tau_{ij}^{sgs}}$ is given by:

$$\widehat{\tau_{ij}^{sgs}} = -\rho \left(\widehat{\widetilde{u_i u_j}} - \widehat{u_i u_j} \right) \quad (41)$$

Now, let us combine the two previous filters in order to define $\widehat{\frown} = \widetilde{\frown}$ and let us apply this latter filter to equation 37; this leads to:

$$\frac{\partial \widetilde{u_i}}{\partial t} + \frac{\partial}{\partial x_j} (\widetilde{u_i u_j}) = -\frac{1}{\rho} \frac{\partial}{\partial x_j} [\widetilde{P} \delta_{ij} - \widetilde{\tau_{ij}} - T_{ij}^{sgs}], \quad (42)$$

where T_{ij}^{sgs} is the SGS stress tensor associated to this third filter $\widetilde{\frown}$ and is defined as:

$$T_{ij}^{sgs} = -\rho (\widetilde{u_i u_j} - \widetilde{u_i} \widetilde{u_j}) = -\rho \left(\widehat{\widetilde{u_i u_j}} - \widehat{\widetilde{u_i}} \widehat{\widetilde{u_j}} \right) \quad (43)$$

Recalling that $\widehat{\frown} = \widetilde{\frown}$, equations 40 and 42 can be combined to establish the following relationship between $\widehat{\tau_{ij}^{sgs}}$ and T_{ij}^{sgs} :

$$T_{ij}^{sgs} = \widehat{\tau_{ij}^{sgs}} - \rho \widehat{\widetilde{u_i u_j}} + \rho \widehat{\widetilde{u_i}} \widehat{\widetilde{u_j}} \quad (44)$$

This equation is known as the Germano identity and can be used to dynamically adapt the constant of any SGS model. As an illustration, its use to determine the Smagorinsky constant is detailed in the following.

Recall first that the Smagorinsky (1963) model for the SGS eddy viscosity corresponding to the filter $\overline{\frown}$ of width Δ reads:

$$\nu_{\text{SGS}} = (C_s \Delta)^2 |\overline{S}|, \quad |\overline{S}| = \sqrt{2 \overline{S_{ij}} \overline{S_{ij}}}. \quad (45)$$

so that the corresponding SGS stress tensor is:

$$\tau_{ij}^{sgs} - \frac{1}{3} \delta_{ij} \tau_{ll}^{sgs} \approx 2 \rho (C_s \Delta)^2 \sqrt{2 \overline{S_{ij}} \overline{S_{ij}}} \overline{S_{ij}}, \quad (46)$$

Assuming that the same constant model C_s holds if the $\widehat{\frown}$ filter is used instead, and noting $\widehat{\Delta}$ the corresponding filter width, one obtains the following expression for T_{ij}^{sgs} :

$$T_{ij}^{sgs} - \frac{1}{3} \delta_{ij} T_{ll}^{sgs} \approx 2 \rho (C_s \widehat{\Delta})^2 \sqrt{2 \widehat{\overline{S_{ij}}} \widehat{\overline{S_{ij}}}} \widehat{\overline{S_{ij}}}, \quad (47)$$

Applying the $\widehat{\frown}$ filter to equation 46 one obtains also:

$$\widehat{\tau_{ij}^{sgs}} - \frac{1}{3} \delta_{ij} \widehat{\tau_{ll}^{sgs}} \approx 2 \rho (C_s \Delta)^2 \sqrt{2 \widehat{\overline{S_{ij}}} \widehat{\overline{S_{ij}}}} \widehat{\overline{S_{ij}}}, \quad (48)$$

Injecting equations 47 and 48 into the Germano identity 44, one obtains:

$$2 \rho (C_s \widehat{\Delta})^2 \sqrt{2 \widehat{\overline{S_{ij}}} \widehat{\overline{S_{ij}}}} \widehat{\overline{S_{ij}}} + \frac{1}{3} \delta_{ij} T_{ll}^{sgs} = 2 \rho (C_s \Delta)^2 \sqrt{2 \overline{S_{ij}} \overline{S_{ij}}} \overline{S_{ij}} + \frac{1}{3} \delta_{ij} \widehat{\tau_{ll}^{sgs}} - \rho \widehat{\widetilde{u_i u_j}} + \rho \widehat{\widetilde{u_i}} \widehat{\widetilde{u_j}} \quad (49)$$

Equation 49 corresponds to five independent scalar equations involving the Smagorinsky model C_s . Most of the time, this indeterminacy is dealt with by choosing the value of C_s

(as a function of space and time) that best satisfies this over-determined system Lilly (1992). Recasting equation 49 in the form:

$$C_s^2 \mathcal{M}_{ij} = \mathcal{N}_{ij} \quad (50)$$

one obtains the following expression for C_s :

$$C_s^2 = \frac{\mathcal{N}_{ij} \mathcal{M}_{ij}}{\mathcal{M}_{ij} \mathcal{M}_{ij}} \quad (51)$$

This procedure often leads to a significant fraction of negative values for C_s^2 , and thus may generate numerical instabilities. A common remedy involves averaging C_s over space but this approach is restricted/justified to simple geometries since the existence of direction of flow homogeneity is required (as in a channel flow). A Lagrangian version of the dynamic Smagorinsky model has been proposed by Meneveau et al. (1996) to allow the computation of complex configurations without direction of flow homogeneity. Very good results have been obtained with this formulation which requires the resolution of two other transport equations Meneveau et al. (1996). The dynamic localization models (constrained or with a transport equation for the kinetic energy) proposed by Ghosal et al. (1995) are in principle applicable to general inhomogeneous flows and do not require spatial averaging. Still, the dynamic procedure is based on the energy transfer between the resolved field and low-pass filtered field. Practically, the width of the filter is Δ for the first field and $\gamma\Delta$ for the second ($\gamma \simeq 2$ is often used). In simple geometries, the filtering operations can be performed very precisely in Fourier space but defining a test filter of width 2Δ in complex geometries may prove to be an issue Jansen (1994). Note however that efficient filters with good commutativity properties can be developed in an unstructured environment (Vasilyev et al., 1998; Marsden et al., 2002; Haselbacher and Vasilyev, 2003). At last recall that the dynamic procedure is general and can virtually be applied to any SGS model to adjust its constant. Notably, it can be applied to any model for the SGS heat flux (see e.g. equation 25) in order to determine λ_{SGS} without assuming a (constant) value for the SGS Prandtl number as in section §3.2.

4 Boundary Conditions

Unsteady computations have to reproduce all the wave propagation phenomena, and dissipative schemes are out of the question from the start. With more accurate schemes, higher demands are put on the boundary conditions and the need is evident of boundary conditions which permit waves to leave the domain without unwanted reflections. Some studies indicate that reflections may be of numerical origin.

Practical applications need various inflow and outflow boundary conditions like non-reflecting inlet or outlet, unsteady inlet with fluctuating velocity fields, as well as wall conditions. These conditions should meet the following criteria:

- The right number of constraints has to be imposed at a given boundary to ensure well-posedness. This number can be derived analytically (Kreiss, 1970; Engquist and Majda, 1977; Higdon, 1986; Gustafsson and Sundstrom, 1978).
- The physics of the problem has to be properly translated into the wave/boundary interactions. For example, with a pressure imposed outlet, an acoustic wave leaving the domain should be transformed into an ingoing one of the same amplitude.
- A numerical implementation of the mathematical and physical statements has to be chosen so as to minimize the numerical perturbations generated at the boundaries. There is clear experimental evidence that backward propagating acoustic waves may trigger an hydrodynamic instability of the Kelvin-Helmholtz type (Rockwell and Naudascher, 1979). If the acoustic wave comes from any physical sound generation process, this interaction leads to a feedback instability. However, if the acoustic wave is induced by an improper boundary treatment, the obtained feedback loop has no physical meaning (Buell and Huerre, 1988; Tam and Auriault, 1996).
- The properties of the initial flow field should become unimportant after a characteristic time of the problem has been computed. This requirement seems obvious for any unsteady or steady computation, but may not be met by certain advanced boundary conditions.

Different boundary condition treatments based on the characteristic approach have been proposed in the literature (Chakravarthy, 1983; Thompson, 1987; Poinso and Lele, 1991; Hirsh, 1990), which handle in various degree the above requirements. Several authors focused essentially on the best way to write a non-reflecting boundary condition for the Euler equations (Giles, 1990; Hayder and Turkel, 1995; Atkins and Casper, 1994; Rudy and Strikwerda, 1980). See Givoli (1991) for a review. It is now commonly accepted (Colonus et al., 1993; Ta'asan and Nark, 1995; Freund, 1997) that a perfect formulation is not reachable for the non-linear case and it has been found necessary to add non physical exit zones onto the computation domain. The objective of this section is to clarify the common points of some characteristic boundary conditions found in literature, as well as the way they differ from an analytical point of view. We want to show on simple unsteady test cases how these formal differences change the results. A general procedure for comparing boundary conditions is provided to explain the numerically observed differences. Section § 4.1 presents the general ideas behind the characteristic approach for the boundary conditions as well as different formulations already available in the literature.

It will be shown that a key difference is the method used to interpret the *variation* of the characteristic variables (also called the amplitude or the strength of the waves). Some ideas are presented about the implementation of these characteristic methods in a general unstructured code. Section § 4.2 shows to what extent the quality of the results for unsteady computations is improved or damaged by the choice of the definition for these variations.

4.1 General formalism

For hyperbolic equations, most advanced boundary treatments make use of the characteristic approach, which is described in many basic articles or textbooks (Hirsh, 1990). Characteristic boundary conditions are based on distinguishing ingoing and outgoing waves at the boundary of the domain. Information carried by outgoing waves is left untouched, while the boundary condition must supply information corresponding to the ingoing waves. This can take the form of e.g. prescribing the strength of ingoing waves, or extrapolating characteristic variables, or Riemann invariants.

The time dependent Euler equations are hyperbolic, and can be reformulated in a set of characteristic advection equations. Let us consider the 3D Euler equations in quasi-linear form:

$$\frac{\partial \mathbf{V}}{\partial t} + \mathbf{A} \frac{\partial \mathbf{V}}{\partial x} + \mathbf{B} \frac{\partial \mathbf{V}}{\partial y} + \mathbf{C} \frac{\partial \mathbf{V}}{\partial z} = \mathbf{0}. \quad (52)$$

In this equation, $\mathbf{V} = (\rho, u, v, w, P)^T$ is the vector of the primitive variables and the matrices \mathbf{A} , \mathbf{B} and \mathbf{C} are defined as:

$$\mathbf{A} = \begin{bmatrix} u & \rho & \cdot & \cdot & \cdot \\ \cdot & u & \cdot & \cdot & 1/\rho \\ \cdot & \cdot & u & \cdot & \cdot \\ \cdot & \cdot & \cdot & u & \cdot \\ \cdot & \gamma P & \cdot & \cdot & u \end{bmatrix} \quad \mathbf{B} = \begin{bmatrix} v & \cdot & \rho & \cdot & \cdot \\ \cdot & v & \cdot & \cdot & \cdot \\ \cdot & \cdot & v & \cdot & 1/\rho \\ \cdot & \cdot & \cdot & v & \cdot \\ \cdot & \cdot & \gamma P & \cdot & v \end{bmatrix} \quad \mathbf{C} = \begin{bmatrix} w & \cdot & \cdot & \rho & \cdot \\ \cdot & w & \cdot & \cdot & \cdot \\ \cdot & \cdot & w & \cdot & \cdot \\ \cdot & \cdot & \cdot & w & 1/\rho \\ \cdot & \cdot & \cdot & \gamma P & w \end{bmatrix}, \quad (53)$$

where γ , ρ , $\vec{v} = (u, v, w)^T$ and P represent the isentropic coefficient, the density, the velocity vector and the static pressure respectively. Each of the matrices \mathbf{A} , \mathbf{B} and \mathbf{C} has its own complete set of real eigenvalues and of right and left eigenvectors, which differ from one matrix to the other. The matrix \mathbf{E}_n defined as $\mathbf{A}n_x + \mathbf{B}n_y + \mathbf{C}n_z$ is introduced, where \vec{n} is an arbitrary unit vector. The eigenvalues matrix obtained by diagonalizing \mathbf{E}_n reads as:

$$\mathbf{\Lambda}_n = \mathbf{L}_n \mathbf{E}_n \mathbf{L}_n^{-1} = \text{diag}(\lambda_n^1, \lambda_n^2, \lambda_n^3, \lambda_n^4, \lambda_n^5) = \text{diag}(u_n, u_n, u_n, u_n + c, u_n - c), \quad (54)$$

where $u_n = \vec{u} \cdot \vec{n}$ and c is the speed of sound. The matrices with left (resp. right)

eigenvectors as rows (resp. columns) \mathbf{L}_n and \mathbf{L}_n^{-1} are given by

$$\mathbf{L}_n = \begin{pmatrix} 1 & 0 & 0 & 0 & -1/c^2 \\ 0 & s_{1x} & s_{1y} & s_{1z} & 0 \\ 0 & s_{2x} & s_{2y} & s_{2z} & 0 \\ 0 & n_x & n_y & n_z & 1/\rho c \\ 0 & -n_x & -n_y & -n_z & 1/\rho c \end{pmatrix}, \text{ and } \mathbf{R}_n = \mathbf{L}_n^{-1} = \begin{pmatrix} 1 & 0 & 0 & \rho/2c & \rho/2c \\ 0 & s_{1x} & s_{2x} & n_x/2 & -n_x/2 \\ 0 & s_{1y} & s_{2y} & n_y/2 & -n_y/2 \\ 0 & s_{1z} & s_{2z} & n_z/2 & -n_z/2 \\ 0 & 0 & 0 & \rho c/2 & \rho c/2 \end{pmatrix}. \quad (55)$$

They relate variations of the characteristic variables \mathbf{W}_n to the variations of the primitive vector \mathbf{V} by:

$$\delta \mathbf{W}_n = \mathbf{L}_n \delta \mathbf{V} \quad \delta \mathbf{V} = \mathbf{L}_n^{-1} \delta \mathbf{W}_n, \quad (56)$$

or in full :

$$\delta \mathbf{W}_n = \begin{bmatrix} \delta W_n^1 \\ \delta W_n^2 \\ \delta W_n^3 \\ \delta W_n^4 \\ \delta W_n^5 \end{bmatrix} = \begin{bmatrix} \delta \rho - \frac{1}{c^2} \delta P \\ \vec{s}_1 \cdot \delta \vec{u} \\ \vec{s}_2 \cdot \delta \vec{u} \\ + \vec{n} \cdot \delta \vec{u} + \frac{1}{\rho c} \delta P \\ - \vec{n} \cdot \delta \vec{u} + \frac{1}{\rho c} \delta P \end{bmatrix} \quad (57)$$

and

$$\delta \mathbf{V} = \begin{bmatrix} \delta \rho \\ \delta u \\ \delta v \\ \delta w \\ \delta P \end{bmatrix} = \begin{bmatrix} \delta W_n^1 + \frac{\rho}{2c} (\delta W_n^4 + \delta W_n^5) \\ s_{1x} \delta W_n^2 + s_{2x} \delta W_n^3 + \frac{n_x}{2} (\delta W_n^4 - \delta W_n^5) \\ s_{1y} \delta W_n^2 + s_{2y} \delta W_n^3 + \frac{n_y}{2} (\delta W_n^4 - \delta W_n^5) \\ s_{1z} \delta W_n^2 + s_{2z} \delta W_n^3 + \frac{n_z}{2} (\delta W_n^4 - \delta W_n^5) \\ \frac{\rho c}{2} (\delta W_n^4 + \delta W_n^5) \end{bmatrix}. \quad (58)$$

Unit vectors \vec{s}_1 and \vec{s}_2 are such that they form with \vec{n} an orthonormal basis $(\vec{n}, \vec{s}_1, \vec{s}_2)$. Note that for each unit vector \vec{n} , a different set of characteristic variables is obtained. Also the choice of right and left eigenvectors influences the scaling of the characteristic variables. The first characteristic variation is proportional to entropy variations, the second and third are related to variations in shear velocity, and the last two represent acoustic disturbances.

The five characteristic variables satisfy a set of convection equations, the compatibility equations, with the speed of propagation given by Eq. (54) and with source terms related to pressure and velocity variations in the (\vec{s}_1, \vec{s}_2) -plane. These equations are obtained by multiplying Eq. (52) with \mathbf{L}_n :

$$\begin{aligned}
\frac{\partial W_n^1}{\partial t} + \vec{u} \cdot \vec{\nabla} W_n^1 &= 0, \\
\frac{\partial W_n^2}{\partial t} + \vec{u} \cdot \vec{\nabla} W_n^2 + \frac{1}{2} c \vec{s}_1 \cdot (\vec{\nabla} W_n^4 + \vec{\nabla} W_n^5) &= 0, \\
\frac{\partial W_n^3}{\partial t} + \vec{u} \cdot \vec{\nabla} W_n^3 + \frac{1}{2} c \vec{s}_2 \cdot (\vec{\nabla} W_n^4 + \vec{\nabla} W_n^5) &= 0, \\
\frac{\partial W_n^4}{\partial t} + (\vec{u} + c\vec{n}) \cdot \vec{\nabla} W_n^4 + c (\vec{s}_1 \cdot \vec{\nabla} W_n^2 + \vec{s}_2 \cdot \vec{\nabla} W_n^3) &= 0, \\
\frac{\partial W_n^5}{\partial t} + (\vec{u} - c\vec{n}) \cdot \vec{\nabla} W_n^5 + c (\vec{s}_1 \cdot \vec{\nabla} W_n^2 + \vec{s}_2 \cdot \vec{\nabla} W_n^3) &= 0.
\end{aligned} \tag{59}$$

In general, these equations are decoupled only in 1D, where the second and third line vanish, with $\vec{s}_1 = \vec{s}_2 = \vec{0}$. In the case of the Navier-Stokes equations, additional source terms appear which are related to the viscous effects.

For boundary conditions, \vec{n} is chosen normal to the considered boundary, either inward or outward. In the following, we take the normal outward, which means that negative speed represents information convected into the computational domain. Positive speed correspond to information leaving the domain, independent of the physical boundary condition. However, the decomposition of the Euler equations into a set of waves with \vec{n} normal to the boundary is a crude and sometimes inadequate assumption (Mazaheri and Roe, 1997).

The ingoing information depends on the physical boundary condition, the numerical evaluation of outgoing waves, the truncation error in the boundary approximation chosen and the way relevant boundary variables are updated. Several methods can be used, which can be classified in different ways. Without being complete, we distinguish:

- Extrapolation methods. Space, time or space-time extrapolation of the conservative/primitive (Griffin and Anderson, 1977; Gottlieb and Turkel, 1978) or characteristic (Yee et al., 1982) variables. This includes e.g. a symmetry condition by annihilating normal velocity, or a wall boundary condition which sets the speed to zero for Navier Stokes equations. Characteristic extrapolation includes the use of Riemann invariants which we will discuss and test here (see sections § 4.1.4 and § 4.2.1).
- Application of boundary conditions at the level of the partial differential equations. This category makes use of information about the characteristics, present in the problem. This can be done in the compatibility relations (Hirsh, 1990), or in the equations of motion (Poinsot and Lele, 1991), with a one-sided discretization. This latter technique is more appropriate for the Navier-Stokes equations, when the boundary conditions have to be separated from the viscous terms. In the following, we will focus on this category, which has in common that the boundary conditions act on *variations*, rather than the variables themselves. It means that the strength of incoming waves is calculated as a function of the physical boundary conditions imposed and the strength of the outgoing waves.

Applying an Euler explicit time discretization to Eq. (52), the update of primitive variables can be written as:

$$\Delta \mathbf{V} = \mathbf{V}^{n+1} - \mathbf{V}^n = -\Delta t \mathcal{R} = -\Delta t \left[\mathbf{A} \frac{\partial \mathbf{V}}{\partial x} + \mathbf{B} \frac{\partial \mathbf{V}}{\partial y} + \mathbf{C} \frac{\partial \mathbf{V}}{\partial z} \right] \quad (60)$$

For a given boundary with normal \vec{n} , the full residual \mathcal{R} in Eq. (60) can be split into a normal part \mathcal{R}_n (involving only normal derivatives) and a tangential part \mathcal{R}_s (involving only derivatives along \vec{s}_1 and \vec{s}_2). E.g., in case $\vec{n} = (1, 0, 0)^t$, that is \vec{n} aligned with the x -axis, $\mathcal{R}_n = \mathbf{A} \partial \mathbf{V} / \partial x$ and $\mathcal{R}_s = \mathbf{B} \partial \mathbf{V} / \partial y + \mathbf{C} \partial \mathbf{V} / \partial z$.

Let us call \mathbf{V}^n the boundary value at time level n , $\delta \mathbf{V}^P$ the predicted boundary update due to the interior scheme, before application of the boundary conditions, $\delta \mathbf{V}_w^P$ the part of $\delta \mathbf{V}^P$ to which the boundary conditions will be applied, and $\delta \mathbf{V}^U = \delta \mathbf{V}^P - \delta \mathbf{V}_w^P$ the part of the boundary update which is not affected by the characteristic boundary conditions. As an example, in methods which identify waves only using terms normal to the boundary, and in the case $\vec{n} = (1, 0, 0)^t$, $\delta \mathbf{V}_w^P$ is the predicted value of $-\Delta t \mathcal{R}_n = -\Delta t \mathbf{A} \partial \mathbf{V} / \partial x$ and $\delta \mathbf{V}^U$ is equal to $-\Delta t \left[\mathbf{B} \frac{\partial \mathbf{V}}{\partial y} + \mathbf{C} \frac{\partial \mathbf{V}}{\partial z} \right]$. Note that $\delta \mathbf{V}^U$ could also contain other contributions like the diffusive terms in the case of the Navier-Stokes equations or the heat release for combustion. The boundary conditions are then applied as follows:

1. Decide the part $\delta \mathbf{V}_w^P$ of the residual to which the boundary conditions are going to be applied to. If it is the full residual, then $\delta \mathbf{V}_w^P = -\Delta t \mathcal{R}$ and $\delta \mathbf{V}^U = 0$.
2. Using Eq. (57), decompose $\delta \mathbf{V}_w^P$, into characteristic variations $\delta W_n^{in,P}$ and δW_n^{out} due to ingoing and outgoing waves, with corresponding primitive variations $\delta \mathbf{V}_w^{in,P}$ and $\delta \mathbf{V}_w^{out}$.
3. Modify the amplitude of the incoming wave(s) $\delta W_n^{in,P}$ corresponding to the physical requirements at the boundary. This gives corrected amplitudes, $\delta W_n^{in,C}$. Note that the outgoing waves δW_n^{out} must be kept as they are. As an example, consider a pressure imposed subsonic outlet, $\delta P = 0$. The characteristic speeds u_n and $u_n + c$ are positive, and the only wave to be affected by the boundary condition is the ingoing acoustic with speed $u_n - c$. Eq. (58) states that $\delta P = \delta W_n^4 + \delta W_n^5$, which gives $\delta W_n^{5,C} = -\delta W_n^4$.
4. Combine the waves $\delta W_n^{in,C}$ and δW_n^{out} , and transform back to primitive variables using \mathbf{L}_n^{-1} , Eq. (58). This gives $\delta \mathbf{V}_w^C$. The boundary point is then updated according to

$$\mathbf{V}^{n+1} = \mathbf{V}^n + \delta \mathbf{V}^U + \delta \mathbf{V}_w^C = \mathbf{V}^n + \delta \mathbf{V}^U + \delta \mathbf{V}^{in,C} + \delta \mathbf{V}^{out}$$

The decomposition of the Euler equations into a set of waves traveling normally to the boundary provides us with a theoretical basis to derive proper boundary condition treatments. However the theory says nothing on the best choice for defining the part of the update related to the waves ($\delta \mathbf{V}_w^P$). It seems that only the *full residual* approach (Thompson, 1990) ($\delta \mathbf{V}_w^P = \delta \mathbf{V}^P$) and the *normal* approach (Thompson, 1987) ($\delta \mathbf{V}_w^P = -\Delta t \mathcal{R}_n$) have been proposed in the literature as a basis of a general procedure to derive boundary conditions for the Euler equations.

4.1.1 Full residual approach

Applying the boundary conditions to the *full residual*, we have $\delta\mathbf{V}^P = -\Delta t\mathcal{R} = \delta\mathbf{V}_w^P$ and $\delta\mathbf{V}^U = 0$, which means that the update becomes $\mathbf{V}^{n+1} = \mathbf{V}^n + \delta\mathbf{V}_w^C = \mathbf{V}^n + \delta\mathbf{V}^{in,C} + \delta\mathbf{V}^{out}$. As soon as the evaluation of \mathcal{R} by the interior scheme leads to $\mathcal{R} = 0$, the strengths of the waves vanish. Therefore, the boundary point does not vary anymore, and steady state is reached. This boundary conditions has been tested with a large variety of physical boundary inlet and outlet conditions, and in a wide range of test cases. Its behavior is very satisfactory. One undesirable side-effect has been found with the simplest non-reflecting boundary condition, Eq. (61), for the case of a shear flow leaving the domain (see section § 4.2.2).

4.1.2 Normal approach

Here, the boundary conditions are applied to the part of the residual related to the normal derivatives, $\delta\mathbf{V}_w^P = -\Delta t\mathcal{R}_n$. It has been proposed by Thompson (1987) for the non-reflecting condition and by Poinso and Lele (1991) as a basis of a general procedure to derive boundary conditions for the Navier-Stokes equations. A part of the residual ($\delta\mathbf{V}^U$) is not touched by the boundary conditions, and therefore, an additional non-characteristic correction is needed.

When the interior scheme evaluation leads to $\mathcal{R} = 0$, the strengths of the waves do not vanish anymore. Take the example of a pressure imposed outlet, and assume that the boundary is at the prescribed pressure. If the normal residual is non-zero (as it is for a Blasius boundary layer, since $\frac{\partial u}{\partial x}$ is not zero), decomposition results in an outgoing characteristic, which has to be matched by an ingoing characteristic to keep the pressure constant.

4.1.3 Non-reflecting boundary conditions

It is straightforward to derive the strength of the incoming waves for physical boundary conditions like an outlet where pressure or Mach number is imposed. Likewise, an inlet with total pressure and temperature and the flow angles, or total temperature and mass flux poses no problem. It is more complicated to design a non-reflecting boundary condition.

The simplest form of this condition is to set the strength of the incoming wave to zero. In 2D, with W^4 the ingoing characteristic for a subsonic outlet, the *full residual* approach gives (Chakravarthy, 1983; Hayder and Turkel, 1995, 1993; Thompson, 1990):

$$\frac{\partial W^4}{\partial t} = 0 \quad (61)$$

whereas the *normal* approach leads to (Thompson, 1987; Poinso and Lele, 1991):

$$(u_n - c) \frac{\partial W^4}{\partial n} = 0 \quad (62)$$

Hirsh (1990) argues that the simple non-reflecting condition, has to be applied to the advection terms of the bicharacteristic equations:

$$(u_n - c) \frac{\partial W^4}{\partial n} + u_s \frac{\partial W^4}{\partial s} = 0. \quad (63)$$

A more elaborate analysis is performed by Engquist and Majda (1977), and translated for practical implementation by Giles (1990). The analysis for the linearized Euler equations is based on a Fourier decomposition of the solution at the boundary, that is decomposition of plane waves in arbitrary directions. Now, the strength of each ingoing Fourier component is set to zero, and consequently, the ingoing waves in the space-time domain are finite. This introduces a dependency of the incoming characteristic on the tangential derivatives at the boundary. For one-dimensional flow, Eq. (61) is recovered. Here we consider the approximate, two-dimensional unsteady formulation Giles (1990), which for a 2D outlet gives:

$$\frac{\partial W^4}{\partial t} = -u_n \frac{\partial W^2}{\partial s} - u_s \frac{\partial W^4}{\partial s}, \quad (64)$$

where u_n and u_s are the normal and tangential velocity at the boundary, and $\partial/\partial s$ denotes the tangential derivative.

Eq. (61), (62), (63) and (64) are all non-reflecting boundary conditions based on characteristic analysis. They do not produce the same results however. This may be explained by formulating all of them in the same framework: indeed, any (non-reflecting) boundary condition can be written either in terms of time derivatives (*temporal form*) or in terms of normal derivative (*spatial form*). These two forms are linked by the compatibility relations, Eq. (59), and imposing a boundary condition on the time derivative can be translated into a condition on the normal derivative and vice versa. An overview of the presented conditions written in their two equivalent forms (*temporal* and *spatial*) is given in table 1. A key reference is used to name each boundary condition. The conversion between the two forms may be obtained with the 2D version of the compatibility relations which for the ingoing characteristic reduces to:

$$\frac{\partial W^4}{\partial t} + (u_n - c) \frac{\partial W^4}{\partial n} + u_s \frac{\partial W^4}{\partial s} + c \frac{\partial W^2}{\partial s} = 0. \quad (65)$$

Name	<i>temporal form</i>	<i>spatial form</i>
Thompson (1990)	$\frac{\partial W^4}{\partial t} = 0$ Eq. (61)	$\frac{\partial W^4}{\partial n} = -\frac{1}{u_n - c} \left\{ u_s \frac{\partial W^4}{\partial s} + c \frac{\partial W^2}{\partial s} \right\}$
Poinsot and Lele (1991)	$\frac{\partial W^4}{\partial t} = - \left\{ u_s \frac{\partial W^4}{\partial s} + c \frac{\partial W^2}{\partial s} \right\}$	$\frac{\partial W^4}{\partial n} = 0$ Eq. (62)
Hirsh (1990)	$\frac{\partial W^4}{\partial t} = -c \frac{\partial W^2}{\partial s}$	$\frac{\partial W^4}{\partial n} = -\frac{u_s}{(u_n - c)} \frac{\partial W^4}{\partial s}$ Eq. (63)
Giles (1990)	$\frac{\partial W^4}{\partial t} = -u_n \frac{\partial W^2}{\partial s} - u_s \frac{\partial W^4}{\partial s}$ Eq. (64)	$\frac{\partial W^4}{\partial n} = \frac{\partial W^2}{\partial s}$

Table 1: Correspondence between the temporal and the spatial form for some non-reflecting boundary conditions. 2D case.

This table provides a way to formally compare these boundary conditions. Of course, the results of a computation depends only on the choice of the boundary (the rows in the table) and not on the form under which it is written (the columns in the table). It is straightforward to derive the 3D version of these correspondences:

Name of the BC	temporal form	spatial form
Thompson (1990)	$\frac{\partial W^5}{\partial t} = 0$	$\frac{\partial W^5}{\partial n} = -\frac{u_{s1}}{u_n - c} \frac{\partial W^5}{\partial s_1} - \frac{u_{s2}}{u_n - c} \frac{\partial W^5}{\partial s_2} - \frac{c}{u_n - c} \frac{\partial W^2}{\partial s_1} - \frac{c}{u_n - c} \frac{\partial W^3}{\partial s_2}$
Poinsot and Lele (1991)	$\frac{\partial W^5}{\partial t} = -u_{s1} \frac{\partial W^5}{\partial s_1} - u_{s2} \frac{\partial W^5}{\partial s_2} - c \frac{\partial W^2}{\partial s_1} - c \frac{\partial W^3}{\partial s_2}$	$\frac{\partial W^5}{\partial n} = 0$
Hirsh (1990)	$\frac{\partial W^5}{\partial t} = -c \frac{\partial W^2}{\partial s_1} - c \frac{\partial W^3}{\partial s_2}$	$\frac{\partial W^5}{\partial n} = -\frac{u_{s1}}{(u_n - c)} \frac{\partial W^5}{\partial s_1} - \frac{u_{s2}}{(u_n - c)} \frac{\partial W^5}{\partial s_2}$
Giles (1990)	$\frac{\partial W^5}{\partial t} = -u_n \frac{\partial W^2}{\partial s_1} - u_n \frac{\partial W^3}{\partial s_2} - u_{s1} \frac{\partial W^5}{\partial s_1} - u_{s2} \frac{\partial W^5}{\partial s_2}$	$\frac{\partial W^5}{\partial n} = \frac{\partial W^2}{\partial s_1} + \frac{\partial W^3}{\partial s_2}$

Table 2: Correspondence between the temporal and the spatial form for some non-reflecting boundary conditions. 3D case.

4.1.4 About the Riemann invariants

The Riemann invariants is the name given to the integrated 1D characteristics variables, under the assumption of isentropic flow (Hirsh, 1990; Anderson, 1982). They are:

$$\begin{aligned}
 R^1 &= \frac{P}{\rho^\gamma} \\
 R^2 &= u_n + \frac{2c}{\gamma - 1} \\
 R^3 &= u_n - \frac{2c}{\gamma - 1}
 \end{aligned} \tag{66}$$

These quantities are constant along the characteristics $dx/dt = u_n$, $dx/dt = u_n + c$ and $dx/dt = u_n - c$ respectively. A main difference in the application of boundary conditions to the Riemann invariants is that the boundary conditions are now imposed on variables rather than on variations. These treatments use directly the predicted and the previous values of the primitive vector to build its corrected value. Another difference is the assumption of isentropic flow which is not made in the treatments described in the previous subsections. An example of the effect of this hypothesis is given in the next section.

4.2 Comparison of non-reflecting BC

As an illustration of the sensibility of unsteady calculations to the boundary conditions used, the non-reflecting formulations described in the previous sections are tested for different academic test cases (see figure 3):

- a 1D acoustic or entropy wave leaving the computation domain through a non-reflecting outlet (section § 4.2.1),
- the establishment of a 2D shear layer in a domain with no velocity at the initial time (section § 4.2.2),

- a two-dimensional vortex leaving the computation domain through a non-reflecting outlet (section § 4.2.3).

The tested formulations are designed as Riemann invariants, Giles (Giles, 1990), Poinso (Poinso and Lele, 1991), Hirsh (Hirsh, 1990) and Thompson (Thompson, 1990) (see table 1 for the definition of these conditions). Except otherwise stated, all the following computations are performed with a second-order centered scheme in space and a third order explicit Runge-Kutta time stepping. No artificial viscosity is used.

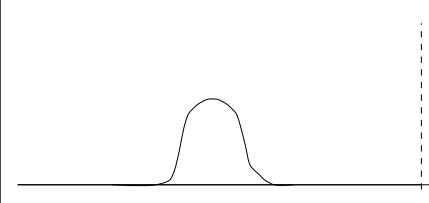
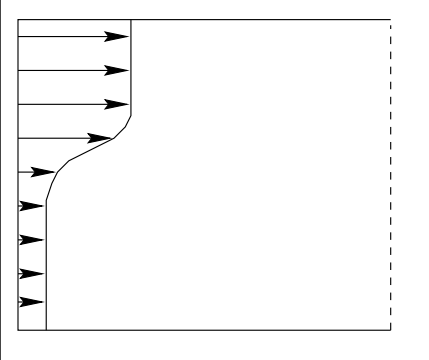
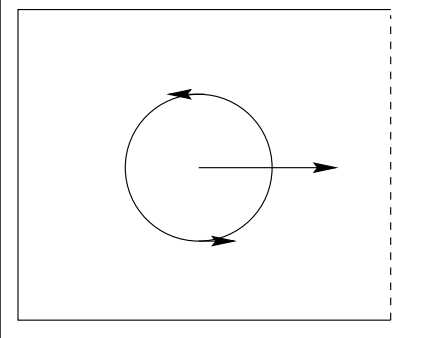
Test cases	Tested conditions
	<ul style="list-style-type: none"> - Riemann invariants - Thompson (1990) - Poinso and Lele (1991) - Hirsh (1990) - Giles (1990)
	<ul style="list-style-type: none"> - Thompson (1990) - Poinso and Lele (1991) - Hirsh (1990) - Giles (1990)
	<ul style="list-style-type: none"> - Poinso and Lele (1991) - Hirsh (1990) - Giles (1990)

Figure 3: Academic test cases for the non-reflecting outlet boundary conditions. The dashed line corresponds to the tested boundary.

4.2.1 One-dimensional cases

A Gaussian perturbation of small amplitude is superimposed to the uniform density field and the other variables are initialized so as to keep energy in only one mode of propagation, either the progressive acoustic one or the entropy one. The mean Mach number is set to

0.25 in both cases and the number of grid points is 201 (uniform mesh). Figures 4 and 5 show the convection of the acoustic perturbation through the evolution of the density at different simulation times. The perturbation leaves the computation domain for $t = 0.5L/(U_0 + c)$, where L is the length of the domain and U_0 is the mean convection velocity. The bottom parts of the figures show that the wave leaves the domain in producing a small amount of numerical perturbation. These sawtooth instabilities have a non-physical negative group velocity of order $-U_0 - c$, in agreement with theoretical analysis (Vichnevetsky and Bowles, 1982). The amplitude of the reflected perturbation is of order of 0.05% of the strength of the outgoing wave, showing that both the Thompson and the Riemann invariants approaches are efficient in this case. Similar results are obtained with the other characteristic treatments cited above. The results for the entropy wave are shown in figures 6 and 7. The characteristic approach produces the same type of result as for the acoustic wave, with the group velocity for the reflected numerical waves which is now of order $-U_0$. The use of the Riemann condition leads to the formation of a regressive acoustic wave ($U_0 - c$) when the entropic wave leaves the computation domain. The density perturbation associated with the reflected wave is even larger than the one related to the outgoing wave. This unacceptable behavior of the Riemann condition is a direct consequence of the isentropic flow assumption used to derive the invariants: this formulation should be used only for isentropic flows. Only characteristic treatments based on the variations of the primitive/characteristic vector will be considered in the following subsections.

4.2.2 Two-dimensional shear-layer

Consider the computation domain defined by $0 < x < 1$ and $0 < y < 1$. The initial condition is uniform for the density and the static pressure, zero for the velocity in the y -direction. For the streamwise velocity, we impose $u(x, y) = U_0(1.5 + \tanh(10(y - 0.5)))$ for $x = 0$, $u(y) = 0$ elsewhere. U_0 corresponds to 0.25 for the Mach number, so that the flow is subsonic everywhere. The Thompson (full residual) characteristic approach is used at the inlet to impose the velocity components and the temperature while a non-reflecting condition is tested at the outlet. The Poincot non-reflecting characteristic condition is used for both $y = 0$ and $y = 1$ to allow acoustic disturbances in the y -direction to leave the domain. The velocity profile is expected to propagate downstream during the computation. The steady solution is obviously $u(x, y) = u(0, y)$ for all x -values. Numerically, several convective times of propagation are simulated before the results are examined. Typical velocity profiles obtained with the Thompson formulation of the outlet boundary are shown in figure 8. Clearly the outlet condition prevents the hyperbolic tangent profile from propagating along the x -direction. Instead, the u -velocity tends to be uniform near the exit. In fact this result is due to the formulation which, by imposing $\partial W_n^4 / \partial t = 0$, forces the temporal evolutions of the streamwise velocity and the pressure to remain nearly proportional. At the initial time, both quantities are uniform at the exit, so that their profiles keep the same shape during the computation if $1/\rho c$ does not depend on y . This feature of the boundary is well recovered by the computation (see figure 9) but is not compatible with the present physical configuration. Instead, the pressure profile should remain uniform and the u -profile should start from zero and tend to the imposed hyperbolic tangent profile at the inlet. The use of the Poincot's approach

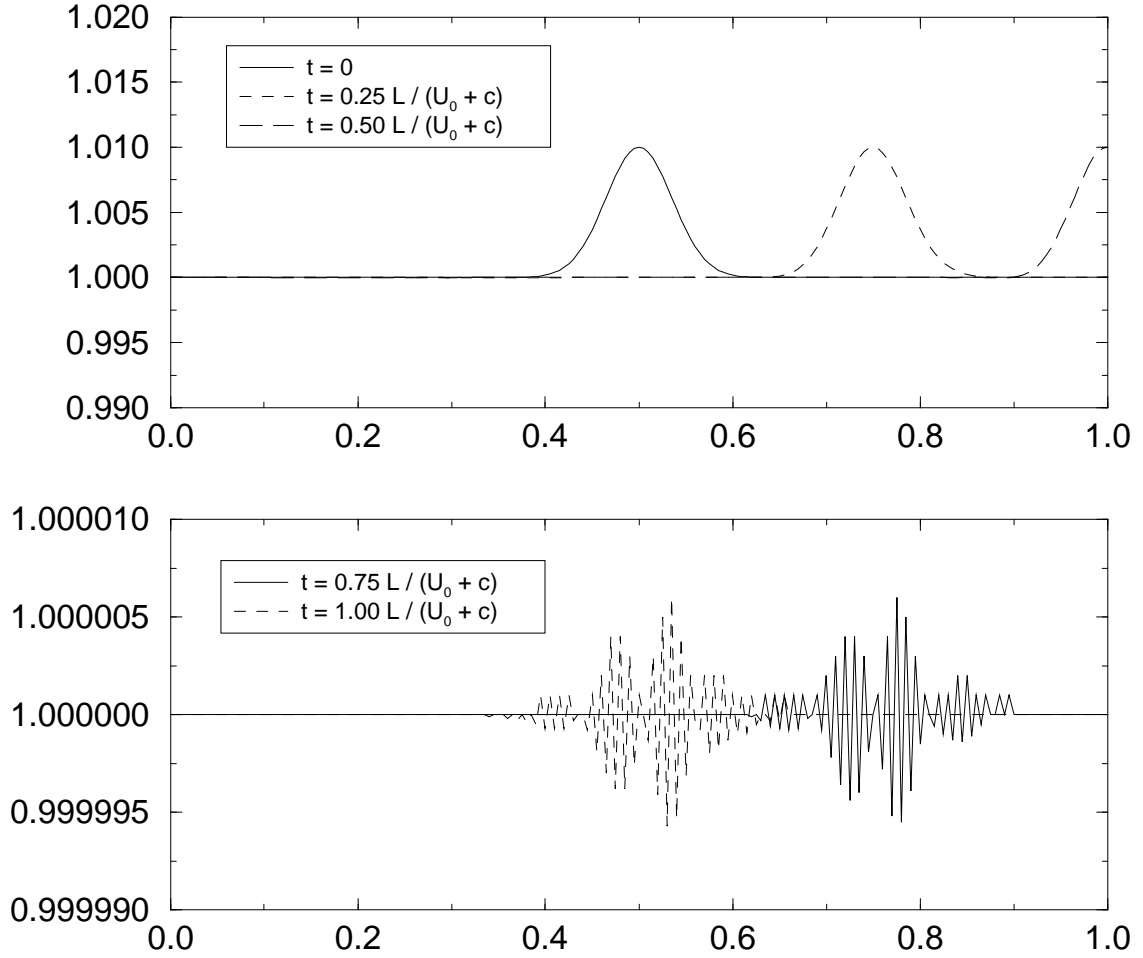


Figure 4: Spatial evolution of density before and after the acoustic wave leaves the domain through the Thompson (1990) (full residual) non-reflecting condition.

for the outlet leads to the correct behavior for the velocity profiles, as shown in figure 10. Indeed, the constraint on the ingoing acoustic wave is now written in terms of spatial gradients, so that the temporal evolutions of the pressure and the velocity at the exit are no more proportional (see table 1). The correct behavior is also obtained for the other characteristic treatments cited above. However the computed physical time needed to reach the steady solution has been found to be greater for the Giles condition than for both the Poinot and the Hirsh formulations. By comparing these boundary conditions in table 1, it appears that three different terms appear in the right-hand-side of their *temporal forms*: $A = u_s \frac{\partial W^4}{\partial s}$, $B = c \frac{\partial W^2}{\partial s}$ and $C = u_n \frac{\partial W^2}{\partial s}$. At least one term is needed to make a boundary condition able to reach the correct steady state. The Poinot's and the Hirsh's conditions leading to equivalent results, the A term above seems not critical for the present test case (this term is the difference between two boundary conditions which give the same results, see table 1). Thus the B term is responsible for the success of the computations with those conditions. One observes also that the C term in the Giles condition is nothing but $\frac{u_n}{c} B$, smaller than B because the test case is subsonic. Thus the observed numerical result (longer relaxation time to the steady state with the Giles treatment) is consistent with the formal comparison of the different boundary conditions.

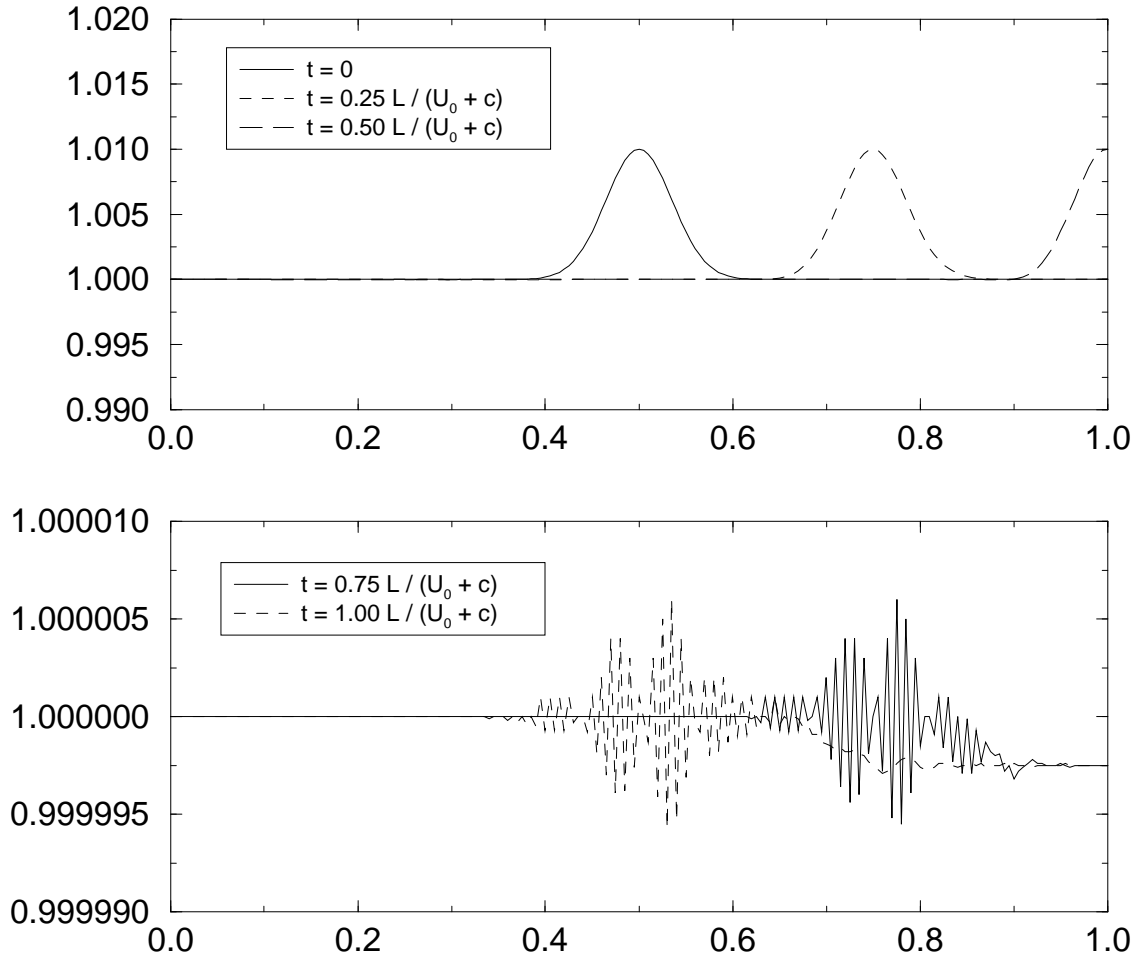


Figure 5: Spatial evolution of density before and after the acoustic wave leaves the domain through a non-reflecting condition based on the Riemann invariants.

Only the formulations proposed by Giles, Poinot and Hirsh have been retained for the next test case.

4.2.3 Two-dimensional vortex

Consider the computation domain defined by $0 < x < 1$ and $0 < y < 1$ and the following stream function:

$$\psi(x, y, t = 0) = \psi_o e^{-\frac{((x-x_o)^2 + (y-y_o)^2)}{a^2}} \quad (67)$$

The corresponding velocity field $u = \frac{\partial \psi}{\partial y}$ and $v = -\frac{\partial \psi}{\partial x}$ defines a steady vortex with center at $x = x_o$ and $y = y_o$ with no vorticity at infinity. ψ_o and a are related to the strength and the size of the vortex respectively. The pressure field associated with this flow is $P = P_o - \rho \psi^2 / a^2$. To define the initial field, a uniform flow ($M = 0.25$) in the streamwise direction is superimposed to the previous vortex flow with $x_o = y_o = 0.5$. Two cases (A and B) have been computed.

Table 3 gives the numerical values of the initial stream function ψ_o , the size of the vortex a and its strength, defined as $\omega_{max} a / U_0$.

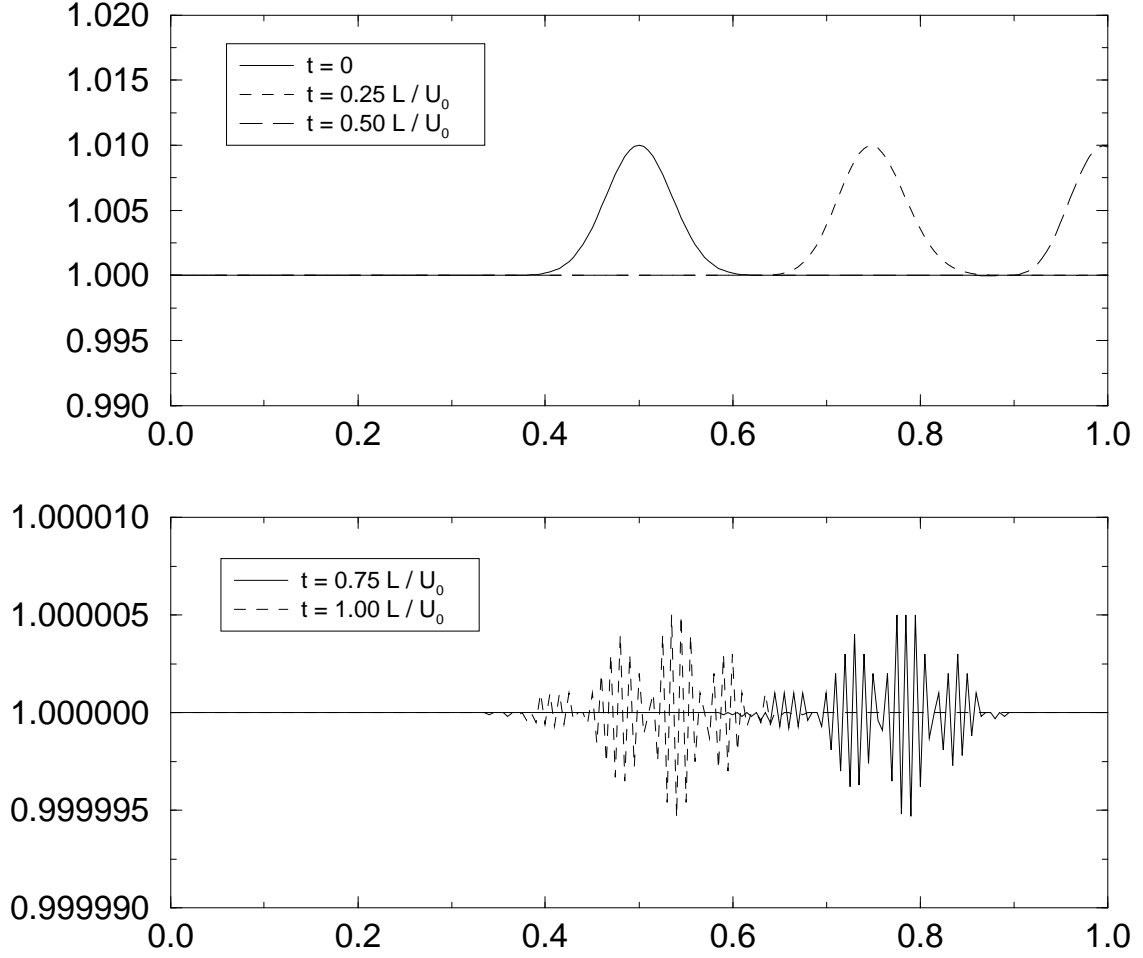


Figure 6: Spatial evolution of density before and after the entropy wave leaves the domain through the Thompson (1990) (full residual) non-reflecting condition.

Case A corresponds to a weak vortex for which the induced velocity is only 1 % of the mean convection velocity U_0 . The second case B stands for a strong vortex for which the induced velocity is 90 % of U_0 . Note that the absolute velocity is always positive for both cases so that the section $x = 1$ is always a subsonic outlet. The Poinso's non-reflecting characteristic condition is used for both $y = 0$ and $y = 1$ to allow the acoustic disturbances in the y -direction to leave the domain. It is also used for $x = 0$ while the tested non-reflecting boundary condition is used for $x = 1$. The vortex is convected downstream during the computation and leaves the domain at time $t = 0.5L/U_0$, where L is the length of the computation domain. With the above presented characteristic formulations for the outlet, the vortex leaves the domain and no vorticity perturbation is produced near the exit.

Case	ψ_o	a	strength
A	0.0005	0.106	0.09
B	0.05	0.159	2.82

Table 3: Strength and size of the computed vortices.

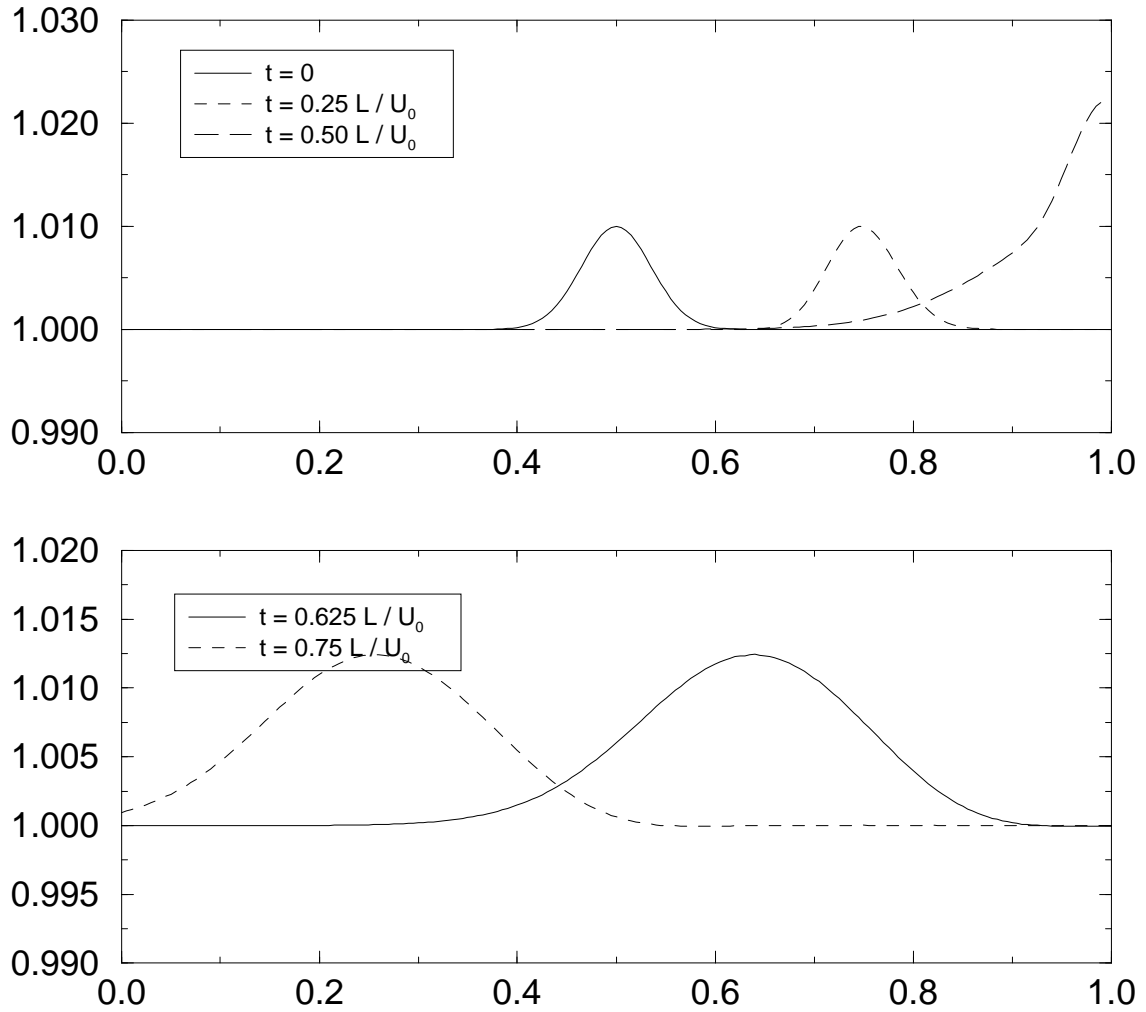


Figure 7: Spatial evolution of density before and after the entropy wave leaves the domain through a non-reflecting condition based on the Riemann invariants.

Figures 11, 12, 13 and 14 show the root-mean-square value of both the vorticity (ω_{rms}) and the divergence (div_{rms}) in the computation domain for Cases A and B. In the first stage of the simulation, both quantities show a plateau because the vortex is still in the domain and there is no dissipation. Around $t = 0.25$, the vortex starts its interaction with the outlet boundary so that the divergence increases. At $t = 0.5$, the center of vortex leaves the computation domain and the level of ω_{rms} sharply decreases. The acoustic perturbations propagate upstream and leave the domain through the different non-reflecting boundaries at the inlet and both the top and the bottom. After $t \simeq 1$, the level of divergence falls to its initial value.

Figures 11 and 12 show the results for the Case A (weak vortex) with the outlet section treated with the (Poinsot and Lele, 1991) and the Giles (1990) formulation respectively.¹ For both formulations, the computed time evolution of ω_{rms} compares well with the analytical one. This latter is the solution of the simple linear convection problem which

¹the non-reflecting boundary condition given by Hirsh (1990) produced results very similar to those obtained with the approach of Poinsot so that the corresponding plots are not shown for clarity.

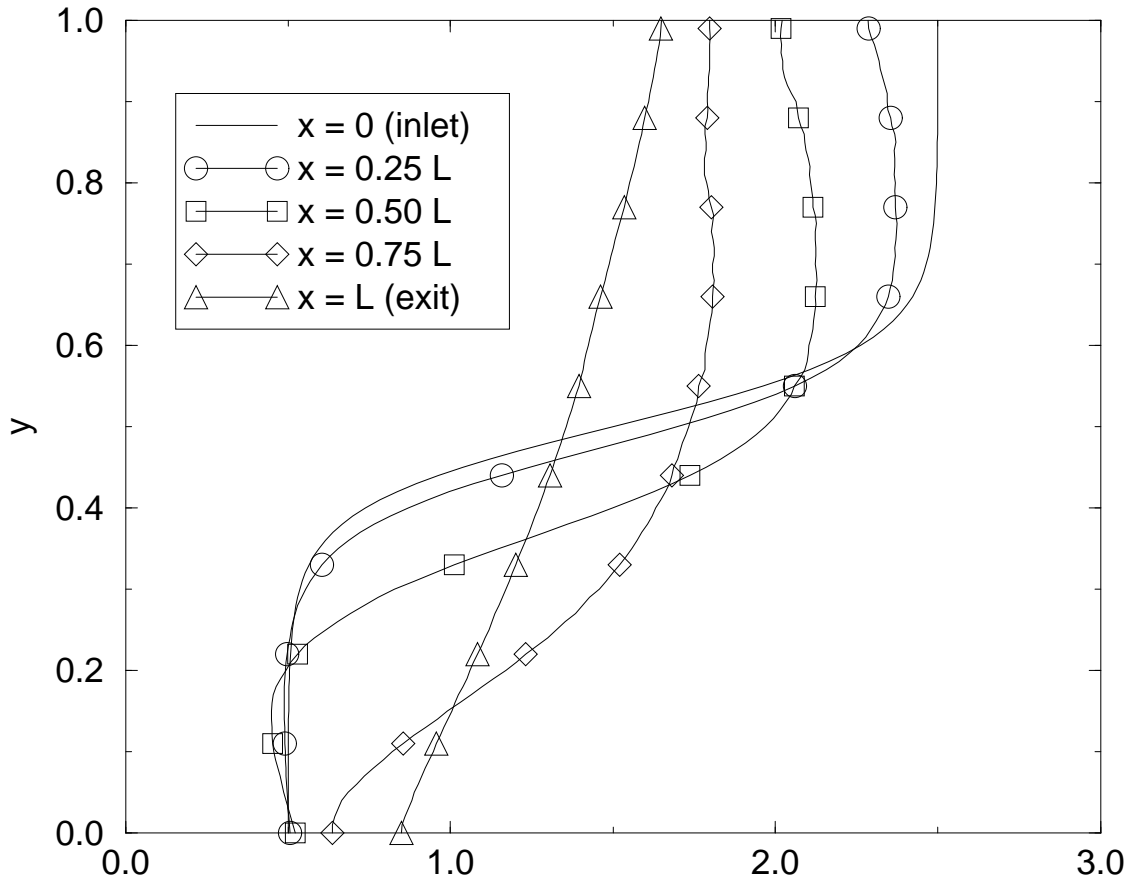


Figure 8: Velocity profiles at different abscissa for the Thompson (1990) (full residual) non-reflecting outlet boundary condition.

is valid as far as the velocity induced by the vortex is small compared to the convection velocity. On the other hand, the treatments produce an amount of dilatation which may be related to the amplitude of the reflected acoustic wave when the vortex leaves the domain (Colonius et al., 1993). A coefficient of acoustic reflection may be defined as the ratio of the maximum of divergence in the computation domain during the exit process to the maximum of vorticity in the incident vortex. It is much smaller for the Giles formulation than for the other one (4 %). Note that for the vortex strength and the spatial resolution considered in Case A, the amount of divergence produced by the Giles exit boundary is of the same order than the initial level of divergence which is related to the truncation error of the second-order spatial scheme used for the computations. As a consequence the reflexion coefficient for this case can hardly be measured except if the resolution is drastically increased. Instead, we preferred to increase the accuracy of the numerical method to check the behavior of the Giles condition in the linear range. Indeed, this condition is exact for the linearized Euler equations (Giles, 1990). It is a second order condition so that the vorticity-acoustic reflexion coefficient should tend to zero as the strength of the vortex does. On the other hand, the first order Poincot condition should produce a nearly constant reflexion coefficient. These features have been well recovered in the present study (see figure 15) by using a sixth-order compact scheme and a third order Runge-Kutta formulation for the time stepping.

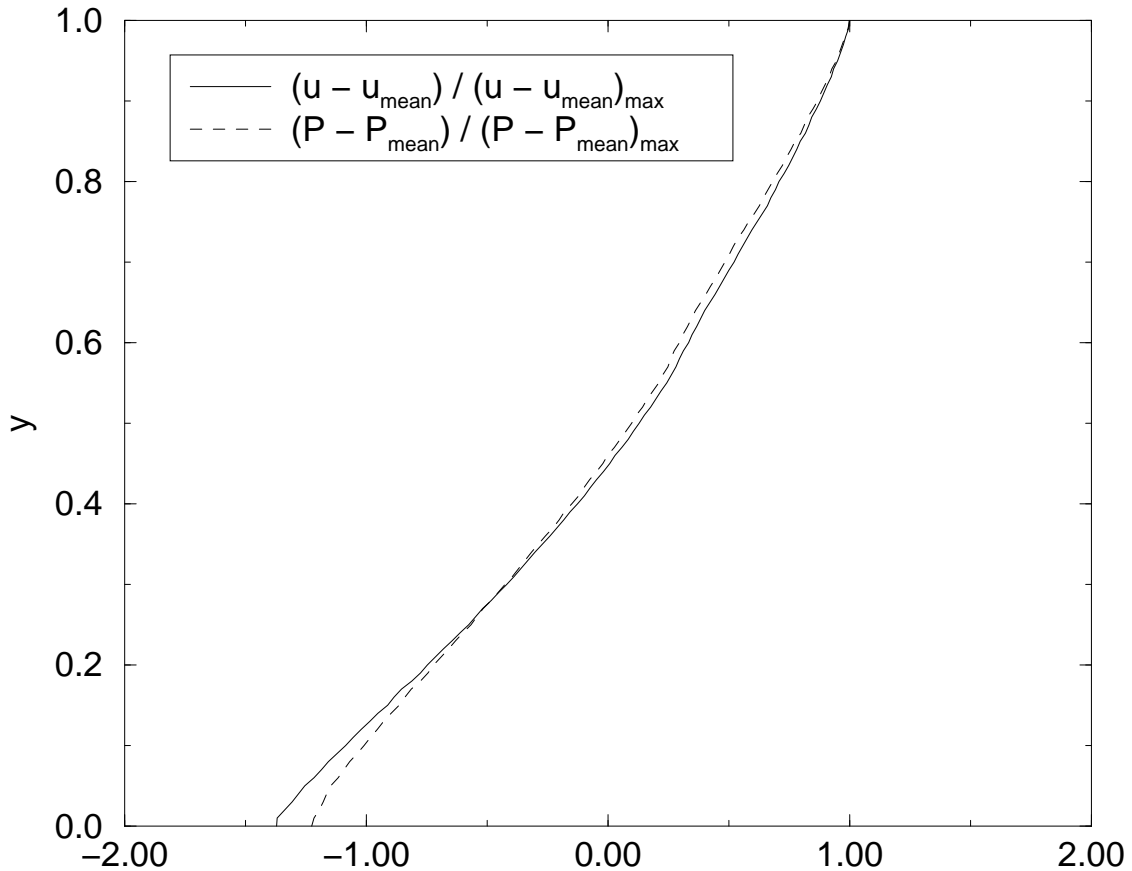


Figure 9: Comparison of the shape of the streamwise velocity and static pressure profiles at the exit plane. The shape of g is defined as $(g - g_{mean}) / (g - g_{mean})_{max}$, where g_{mean} is the mean value of g at the exit.

Figures 13 and 14 correspond to the case B. Even for the non-linear vortex, the decrease of the vorticity in the computation domain is well reproduced by both boundary treatments. Note that the 'exact' solution in these figures correspond to a simulation with a domain of length 2, the root-mean-square of vorticity being computed over the first half of it. In terms of reflected acoustic wave, the difference between the two boundary treatments decreases when the strength of the vortex increases, as suggested by figure 15. For case B, both conditions lead to the same order of reflexion coefficient (around 4 % for both). This is due to non-linear effects which are not properly accounted for, whatever the boundary formulation. A way to overcome this difficulty is to insert a buffer region before the exit section, so as to make the perturbation linear before it interacts with the boundary (Colonus et al., 1993).

4.3 More about BC treatments

4.3.1 Linear relaxation

The classical characteristic formulation is widely used since it provides a theoretical basis to derive proper boundary condition treatments, following the steps described in section §4.1. Consider the case of a subsonic outlet where the static pressure is known. Such a

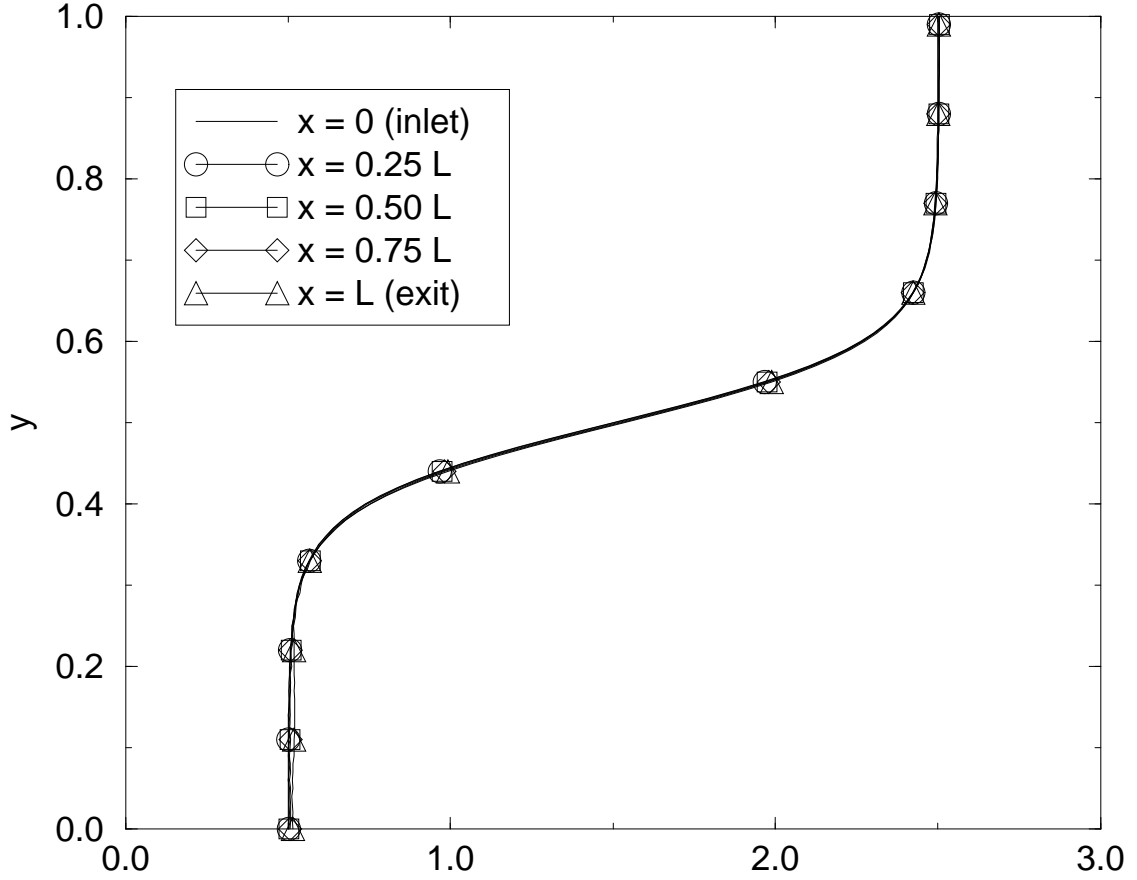


Figure 10: Velocity profiles at different abscissa for the Poinso and Lele (1991) non-reflecting outlet boundary condition.

condition must be based on the relationship between the pressure variations δP and the variations of the characteristics variables δW_n^4 and δW_n^5 . From Eqs. (58) one obtains:

$$\delta P = \frac{\rho c}{2}(\delta W_n^4 + \delta W_n^5) \quad (68)$$

which may be rewritten as:

$$\delta W_n^5 = -\delta W_n^4 + \frac{2}{\rho c}\delta P \quad (69)$$

Note that this boundary condition is fully reflecting acoustically: any physical or numerical perturbation generated during the calculation cannot leave the computational domain. To ensure the stability of the simulation, one often makes use of dissipative schemes in order to damp the perturbations that cannot be evacuated through the boundaries. However, using dissipative numerical schemes for calculating unsteady flows may lead to erroneous results (Colin and Rudgyard, 2000). Experience proves that it may be sufficient, and safer numerically, to use a boundary treatment that is not fully reflecting. In order to built an essentially non-reflecting boundary condition where the ingoing wave does not depend on the outgoing wave, we write, instead of Eq. (69) :

$$\delta W_n^5 = +\frac{2}{\rho c}\delta P \quad (70)$$

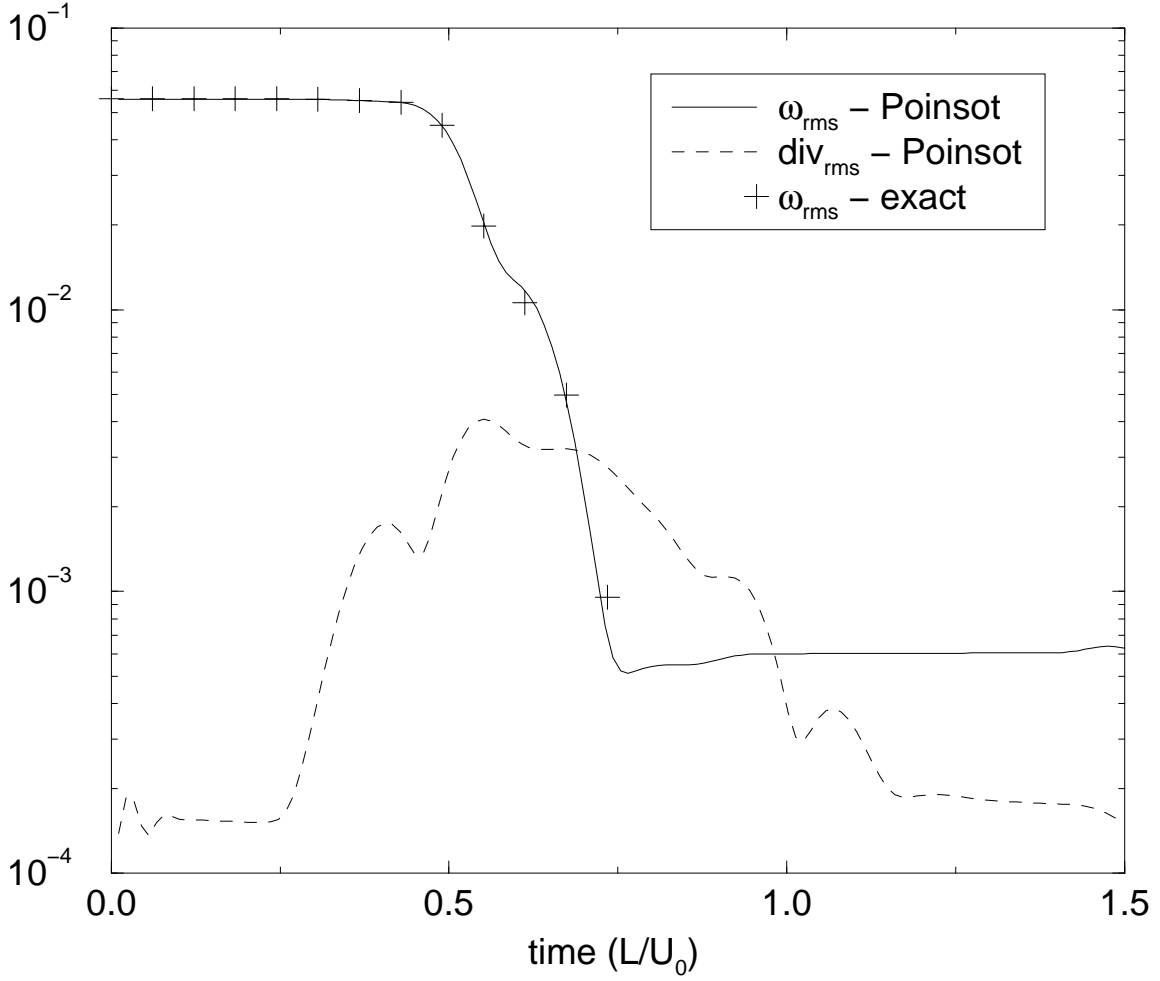


Figure 11: Time evolutions of the rms of vorticity and divergence during the exit of a linear vortex through a non-reflecting subsonic outlet condition. Case A - Treatment of Poincot.

In the case of a fully non-reflecting condition, we would have no acoustic wave entering the domain, that is $\delta W_n^5 = 0$. However, it turns out that such condition is ill-posed and might lead to very large uncontrolled pressure drift. To avoid this, one relaxes the pressure at the boundary P^B toward the target value P^t by choosing $\delta P = \overline{\alpha_P}(P^t - P^B)$, leading to :

$$\delta W_n^5 = \overline{\alpha_P} \frac{2}{\rho c} (P^t - P^B) \quad (71)$$

In order to make the effect of the dimensionless relaxation parameter $\overline{\alpha_P}$ independent on the time step Δt , it is preferable to take instead :

$$\delta W_n^5 = \alpha_P \frac{2}{\rho c} (P^t - P^B) \Delta t \quad (72)$$

where the relaxation parameter α_P is homogeneous to a frequency. In absence of wave reflexion from the domain (that is if $\delta W_n^4 = 0$), this choice for the variation of the ingoing characteristic variable δW_n^5 has the effect to move the pressure at the boundary from the value P^B to the value $P^B + \alpha_P (P^t - P^B) \Delta t$, which is closer to the target value P^t provided

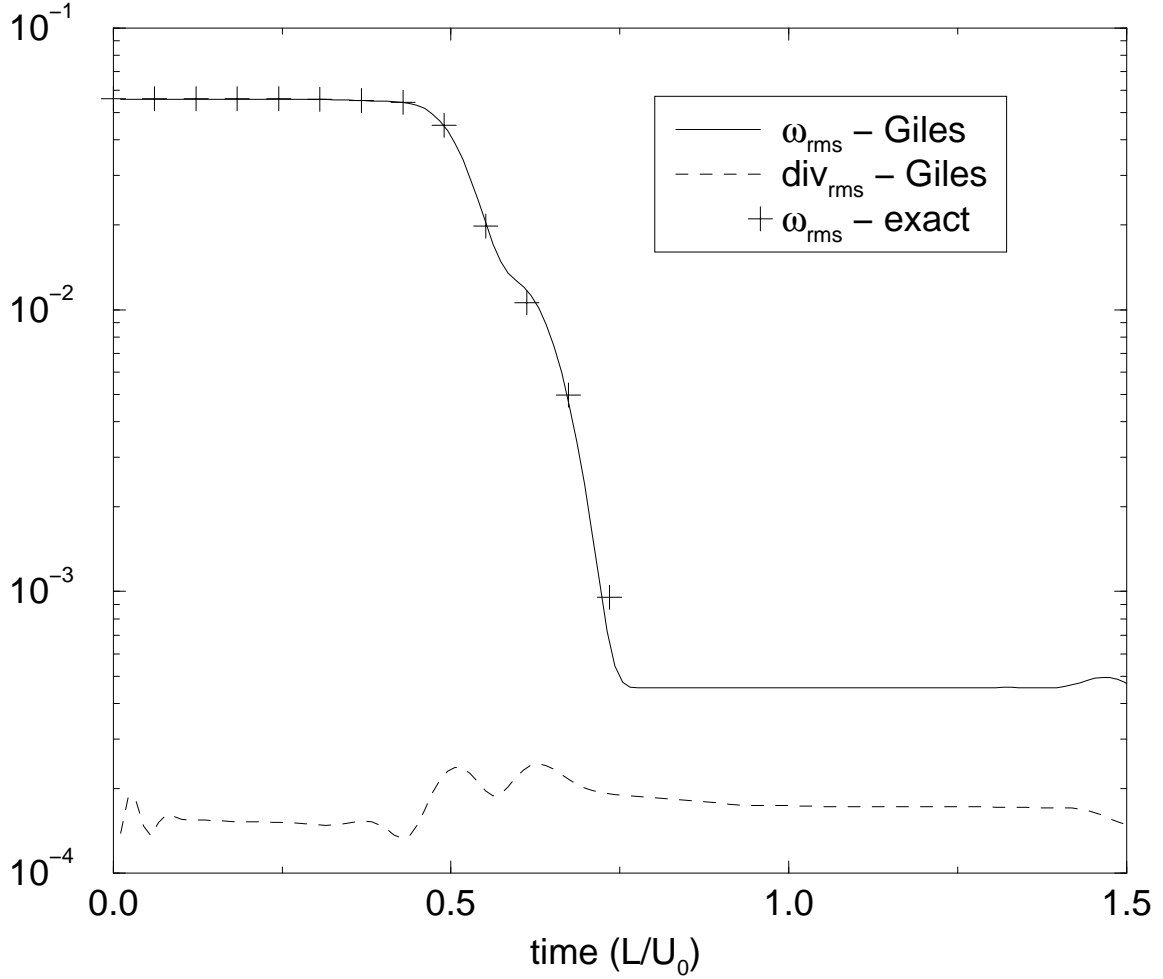


Figure 12: Time evolutions of the rms of vorticity and divergence during the exit of a linear vortex through a non-reflecting subsonic outlet condition. Case A - Treatment of Giles.

the relaxation coefficient is not too large. The net effect is to avoid large pressure drift if α_P is large enough (to compensate the causes of the drift). This is similar to what proposed Rudy and Strikwerda (1980). They showed that the relaxation coefficient is related to the characteristic size of the domain and the characteristic Mach number. The condition (72) is virtually non-reflecting if P^B is close to P^t but prevents the computed pressure from being too different from the reference. Note that, contrary to the full reflecting formulation (69), equation (72) does not guaranty that P^B is strictly equal to P^t . It can be shown that the inclusion of a relaxation term as in equation 72 makes the boundary transparent only for perturbation whose frequency is larger than a cut-off frequency f_c which can be related to the relaxation coefficient α_P . A simple analytical model allows to show that $f_c = \alpha_P/4\pi$ (Selle et al., 2004).

4.3.2 Approximate boundary conditions

The purpose of any characteristic boundary condition is to prescribe proper value(s) of the ingoing characteristic variable(s) so that the expected physical boundary condition is

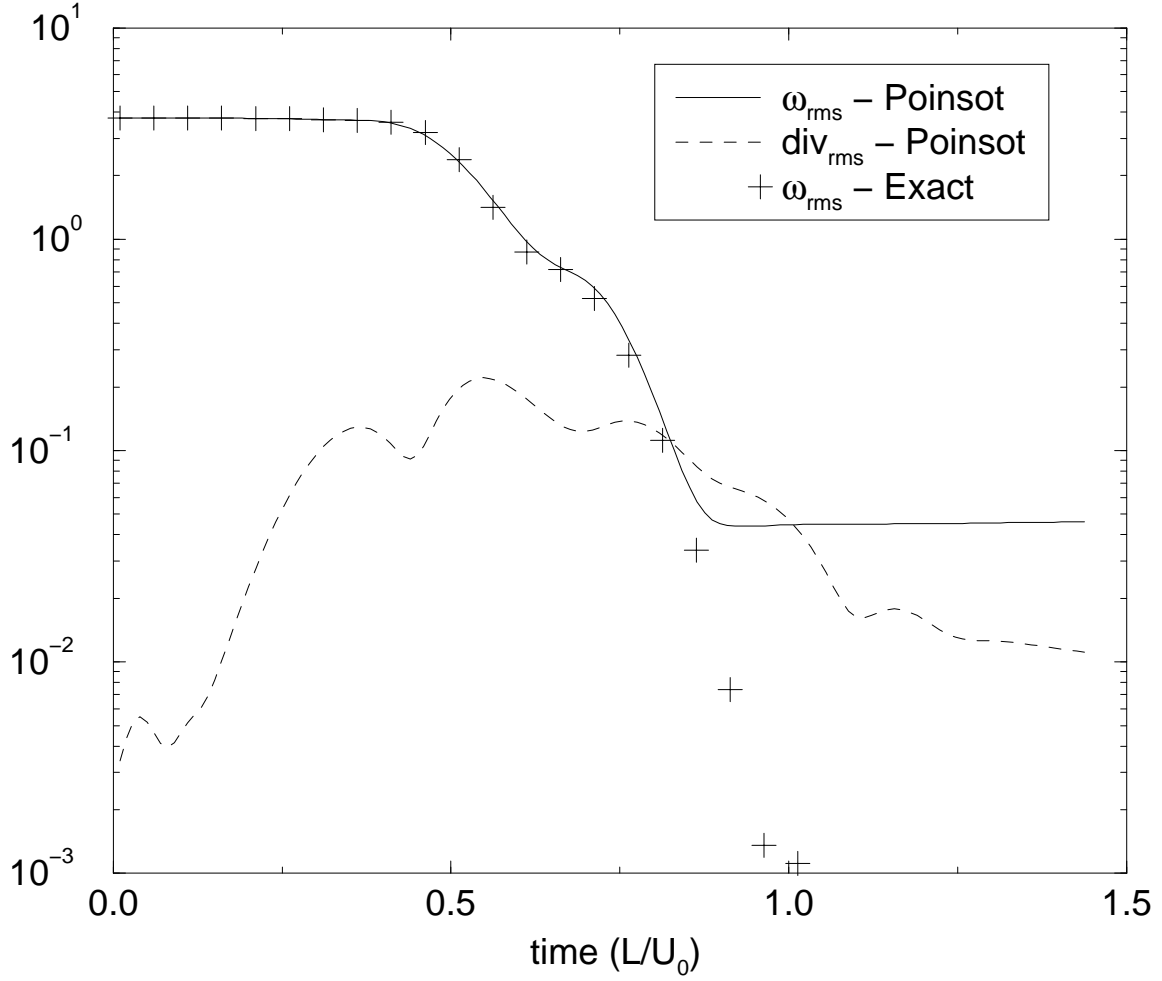


Figure 13: Time evolutions of the rms of vorticity and divergence during the exit of a non-linear vortex through a non-reflecting subsonic outlet condition. Case B - Treatment of Poincot.

obtained. The linear relaxation methodology described above can be used to construct any kind of (well-posed) inlet/outlet boundary condition. A few examples are provided below

- **Mass flow rate 'imposed' outlet:** One assumes that the normal mass flow rate ρu_n is known at a subsonic outlet. From Eqs. (58) and (57) one obtains:

$$\delta\rho u_n = \frac{\rho}{2}(1 + M_n)\delta W_n^4 - \frac{\rho}{2}(1 - M_n)\delta W_n^5 + u_n\delta W_n^1 \quad (73)$$

which may be rewritten as:

$$\delta W_n^5 = \frac{1}{1 - M_n} \left[(1 + M_n)\delta W_n^4 + \frac{2}{\rho}u_n\delta W_n^1 - \frac{2}{\rho}\delta\rho u_n \right] \quad (74)$$

In these equations, M_n stands for the normal Mach normal at the boundary. Note that for an outlet, u_n is positive and M_n could tend toward 1 for high subsonic flows. As a consequence, this boundary condition becomes ill-posed in the transonic

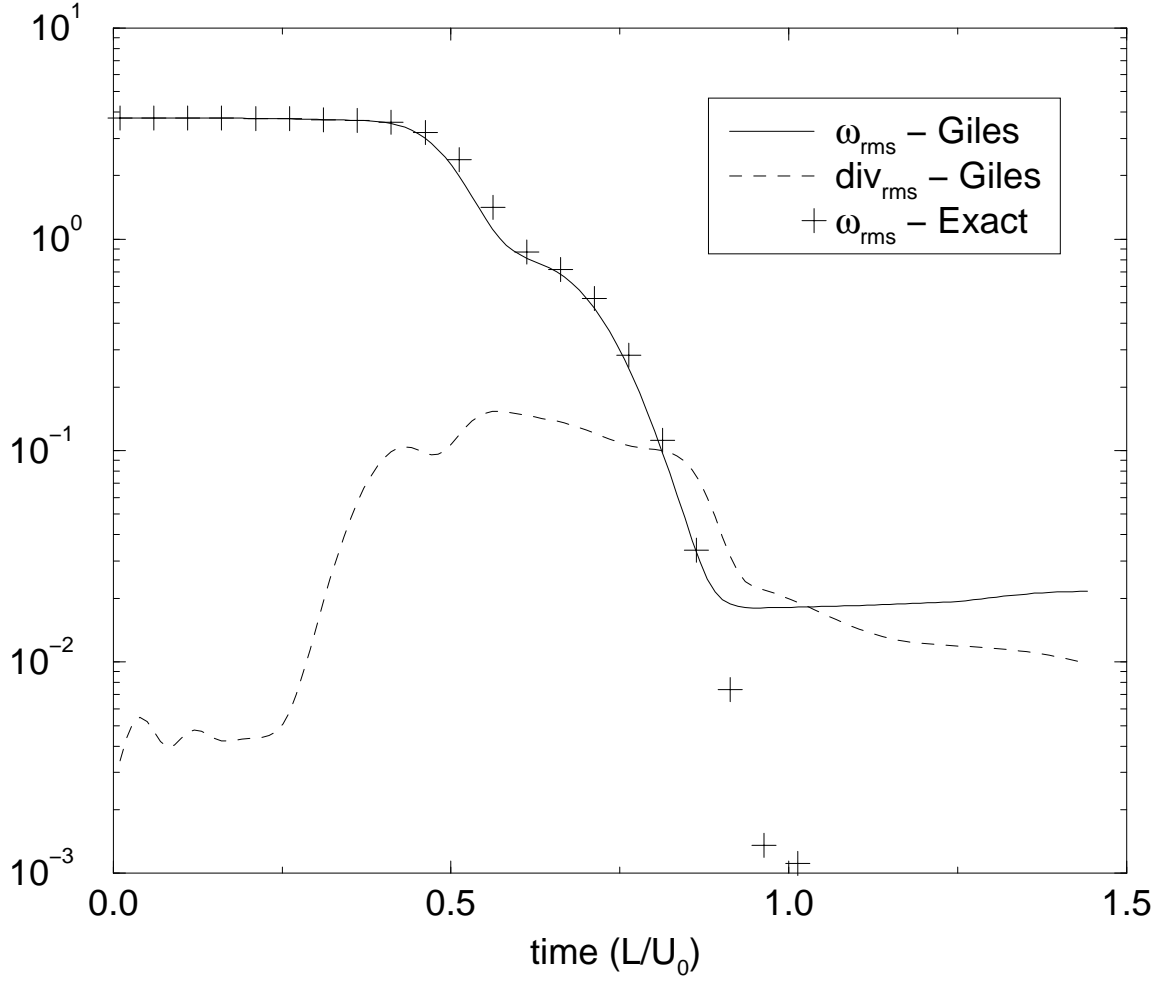


Figure 14: Time evolutions of the rms of vorticity and divergence during the exit of a non-linear vortex through a non-reflecting subsonic outlet condition. Case B - Treatment of Giles.

regime (which could have been expected since the flow rate through a choked nozzle is imposed from the upstream conditions only). As in section §4.3.1, the essentially non-reflecting outlet with relaxation toward the target value ρu_n^t is obtained by assuming that the incoming wave does not depend on the outgoing characteristics:

$$\delta W_n^5 = \frac{2\alpha_{\rho u_n}}{\rho(1 - M_n)}(\rho u_n^t - \rho u_n^B) \quad (75)$$

- **Inlets with velocity and temperature 'imposed'**: It is common use to impose the velocity vector and static temperature at subsonic inlets. Such condition should be based on the relationships between the velocity and temperature variations and the variations of the characteristics variables. From Eqs. (57) and (58) one obtains

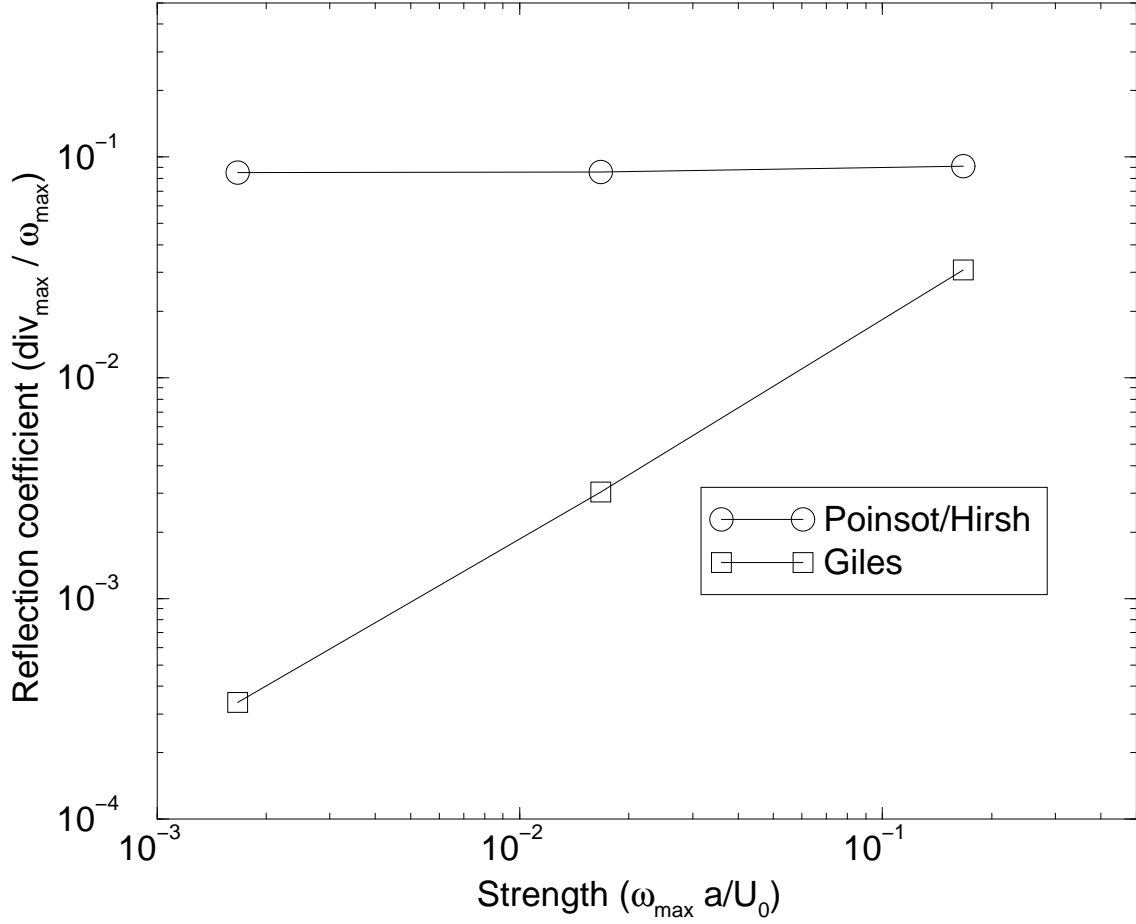


Figure 15: Coefficient of acoustic reflection as a function of the amplitude of the incident vortex. Comparison between a first order (Poinot, Hirsh) and a second order (Giles) condition in the linear range. Results from a code based on a sixth-order compact scheme.

(using the state equation to express $\delta T = T \delta P / P - T \delta \rho / \rho$):

$$\begin{bmatrix} \delta W_n^1 \\ \delta W_n^2 \\ \delta W_n^3 \\ \delta W_n^5 \end{bmatrix} = \begin{bmatrix} \frac{(\gamma-1)\rho}{c^2} [-C_p \delta T - c \delta u_n + c \delta W_n^4] \\ \delta u_{t_1} \\ \delta u_{t_2} \\ \delta W_n^4 - 2\delta u_n \end{bmatrix} \quad (76)$$

The essentially non-reflecting inlet relaxation toward the target values u_n^t , $u_{t_1}^t$, $u_{t_2}^t$ and T^t is obtained by making the incoming waves independent on the outgoing one (δW_n^4):

$$\begin{bmatrix} \delta W_n^1 \\ \delta W_n^2 \\ \delta W_n^3 \\ \delta W_n^5 \end{bmatrix} = \begin{bmatrix} \frac{(\gamma-1)\rho}{c^2} [-C_p \alpha_T (T^t - T^B) - c \alpha_{u_n} (u_n^t - u_n^B)] \Delta t \\ \alpha_{u_t} (u_{t_1}^t - u_{t_1}^B) \Delta t \\ \alpha_{u_t} (u_{t_2}^t - u_{t_2}^B) \Delta t \\ -2\alpha_{u_n} (u_n^t - u_n^B) \Delta t \end{bmatrix} \quad (77)$$

- **Inlets with mass flow rate and total temperature 'imposed'**: This is a variant of the previous condition. Similarly, the starting point is the relationships

between the mass flow rate and total temperature variations and the variations of the characteristics variables. From Eqs. (57) and (58) one obtains (using the state equation to express δT):

$$\begin{bmatrix} \delta \rho u_n \\ \delta \rho u_{t_1} \\ \delta \rho u_{t_2} \\ \delta T_t \end{bmatrix} = \begin{bmatrix} \frac{\rho}{2}(1+M_n)\delta W_n^4 - \frac{\rho}{2}(1-M_n)\delta W_n^5 + u_n\delta W_n^1 \\ \rho\delta W_n^2 + u_{t_1}\delta W_n^1 + \frac{\rho}{2}M_{t_1}(\delta W_n^4 + \delta W_n^5) \\ \rho\delta W_n^3 + u_{t_2}\delta W_n^1 + \frac{\rho}{2}M_{t_2}(\delta W_n^4 + \delta W_n^5) \\ \frac{1}{C_p} \left[u_{t_1}\delta W_n^2 + u_{t_2}\delta W_n^3 - \frac{c^2}{\rho(\gamma-1)}\delta W_n^1 + \frac{1}{2}(c+u_n)\delta W_n^4 + \frac{1}{2}(c-u_n)\delta W_n^5 \right] \end{bmatrix} \quad (78)$$

where M_{t_1} and M_{t_2} are the Mach numbers in the \vec{t}_1 and \vec{t}_2 directions respectively. With some algebra, Eqs. (78) can be inverted to provide the following expressions for the ingoing waves :

$$\begin{bmatrix} \delta W_n^1 \\ \delta W_n^2 \\ \delta W_n^3 \\ \delta W_n^5 \end{bmatrix} = \begin{bmatrix} \frac{1}{\Delta} \left[\frac{\rho(\gamma-1)(1-M^2)}{c} \delta W_n^4 + S_1 \right] \\ \frac{1}{\Delta} \left[-\gamma M_{t_1} \delta W_n^4 + S_2 \right] \\ \frac{1}{\Delta} \left[-\gamma M_{t_2} \delta W_n^4 + S_3 \right] \\ \frac{1}{\Delta} \left[(1 + \gamma M_n + (\gamma - 1)M^2) \delta W_n^4 + S_4 \right] \end{bmatrix} \quad (79)$$

where $\Delta = 1 - \gamma M_n + (\gamma - 1)M^2$ and the terms S_1 , S_2 , S_3 and S_4 are equal to :

$$\begin{bmatrix} S_1 \\ S_2 \\ S_3 \\ S_4 \end{bmatrix} = \begin{bmatrix} \frac{\gamma-1}{c} \left[-(1-M_n) \left(\frac{\rho C_p}{c} \delta T_t - M_{t_1} \delta \rho u_{t_1} - M_{t_2} \delta \rho u_{t_2} \right) - (1-M_n - M_{t_1}^2 - M_{t_2}^2) \delta \rho u_n \right] \\ \frac{1}{\rho} \left[(\gamma-1)M_{t_1} \left(\frac{\rho C_p}{c} \delta T_t + (1-M_n - M_s^2) \delta \rho u_n \right) + (1-\gamma M_n + (\gamma-1)M_n^2) \delta \rho u_{t_1} \right] \\ \frac{1}{\rho} \left[(\gamma-1)M_{t_2} \left(\frac{\rho C_p}{c} \delta T_t + (1-M_n - M_s^2) \delta \rho u_n \right) + (1-\gamma M_n + (\gamma-1)M_n^2) \delta \rho u_{t_2} \right] \\ -\frac{2}{\rho} \left[M_n(\gamma-1) \left(\frac{\rho C_p}{c} \delta T_t - M_{t_1} \delta \rho u_{t_1} - M_{t_2} \delta \rho u_{t_2} \right) + (1+(\gamma-1)M_s^2) \delta \rho u_n \right] \end{bmatrix} \quad (80)$$

where $M_s^2 = M_{t_1}^2 + M_{t_2}^2$.

4.3.3 Integral boundary conditions

The above mentioned boundary treatments require the *pointwise* knowledge of the physical quantity to be imposed at the boundary. For example, consider an isentropic subsonic inlet where the velocity is prescribed, the tangential component being zero. Following the previous reasoning, the following relationship should be used to compute the incoming acoustic wave if the approximate boundary is to be used:

$$\delta W_n^5 = -2\alpha_u (u_n^B - u^t) \Delta t, \quad (81)$$

However, pointwise information about u^t is not always available and the knowledge of the bulk velocity u_{bulk}^t is often less challenging. Integrating the RHS of equation (81) over the boundary B one obtains an integral, approximate boundary condition (Nicoud and Schönfeld, 2002):

$$\delta W_n^5 = -2\alpha_u \left(\frac{1}{S_B} \int_B u_n^B dS_B - u_{\text{bulk}}^t \right) \Delta t, \quad (82)$$

where S_B is the area of B . In this formulation, the incoming acoustic wave depends only on *time* and drives the total flow rate entering the domain through B . The shape of

the velocity profile comes out from the terms not modified by the boundary treatment, *i.e.* $\delta \mathbf{V}^U$ in section §4.1. Note that the integral term in (82) should be assessed at each iteration of the simulation and the input u_{bulk} is a function of time only.

The performance of the above treatment is illustrated in figure 4.3.3. which displays the results from an unsteady Poiseuille flow computation. The averaged bulk Reynolds number is $Re_h = 870$ with h half the channel cross section. The length of the straight channel is $40h$. The unsteady flow is pulsated at frequencies defined by the Womersley number $Wo = h\sqrt{\omega/\nu} = 15$ with ω the pulsation of the flow rate variation. The maximal amplitude is 45% of the mean flow rate. At the channel inlet the integral values of both the flow rate and the temperature are imposed, while at the outlet only the integral value of the flow rate is imposed. The velocity profiles at the inlet and outlet sections at three different instances are displayed in figure 4.3.3. The velocities are scaled by the mean flow velocity $\langle U_{\text{bulk}} \rangle$. The CFD results are compared to the analytical solution (Womersley, 1955) obtained by assuming no dependence in the streamwise direction in a channel submitted to a pressure gradient of the form $\nabla P = \nabla P_0 + \nabla P_1 \exp(j\omega t)$, that is:

$$u(y, t) = -\frac{\nabla P_0}{\mu}(h^2 - y^2) + \mathcal{R} \left[j \frac{\nabla P_1}{\rho\omega} \left(1 - \frac{\cos(\alpha y/h)}{\cos(\alpha)} \right) \right]$$

where y is the normal coordinate and $\alpha = Wo \exp(3j\pi/4)$.

From the results, it appears that the application of sucking outlet conditions is simpler to realize than imposing 'blowing' inlet conditions. This is because the time scale of the diffusion terms in the normal (to the wall) direction is larger than the time scale of the unsteadiness (the Womersley number is a measure of the ratio between these two characteristic times). For smaller values of Wo , this is no longer the case and the results at the inlet improve. In the limit $Wo \rightarrow 0$, the integral boundary treatment allows to recover exactly the parabolic (Poiseuille) profile.

The concept of integral boundary condition can easily be extended to any well-posed subsonic inlet or outlet characteristic based boundary condition, such as those described in section §4.3.2. For example, it is possible to control the bulk pressure at a subsonic outlet boundary, a feature which proves useful when computing swirled flows where the static pressure in planes normal to the main stream is not constant.

4.3.4 Advanced non-reflecting conditions

The formalism presented in section § 4.1 constitutes the basis of the characteristic-based boundary treatments. Given the sensibility of the results to the 'details' of the boundary conditions (see section §4.2), many studies have been published in the recent years to propose improvements. One issue that is often addressed is related to the spurious pressure oscillations that the standard non-reflecting boundary conditions create when applied to turbulent flows. For example, Polifke et al. (2006) proposed to identify plane waves and a slight modification of the relaxation term (as in equation 81) in order to make the approximate non-reflecting condition exactly transparent for all the frequencies, at least for plane waves traveling normally to the boundary. Prosser (2005) performs an analysis of the characteristics used to define non-reflecting boundary conditions. The analysis is conducted in terms of a low Mach number asymptotic series and allows a better understanding of the reason why spurious pressure oscillations are generated. From the Mach

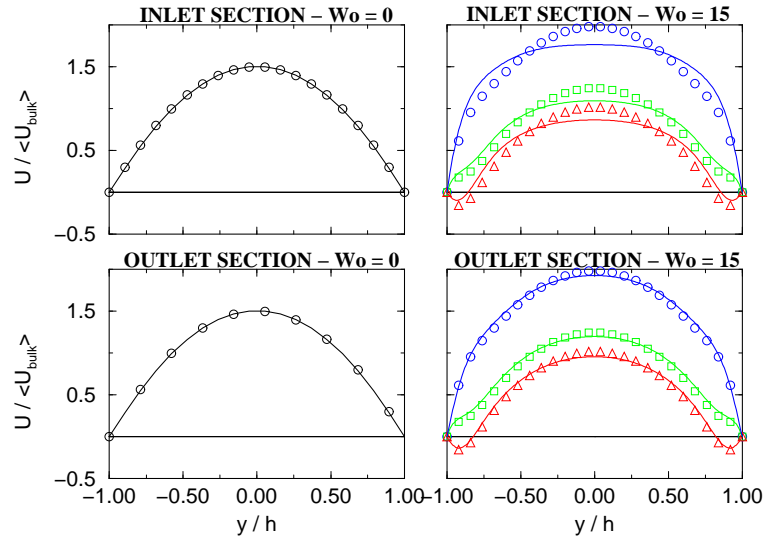


Figure 16: Velocity profiles for steady (left column) and unsteady (right column) Poiseuille flow, at inlet (top row) and outlet (bottom row). Lines indicate CFD calculations, symbols correspond to the analytical solution. Three different phases (0, 70 and 180 degrees) are shown for the case $Wo = 15$.

number expansion, and related scale separation, an improved boundary treatment can be formulated, which is virtually transparent to acoustic waves and allows the prescription of turbulent vortical fluctuations. Characteristic-based boundary treatments have also been proposed to handle more complex situations such as the subsonic flow of multi-species gaseous mixtures (Baum et al., 1994; Okong'o and Bellan, 2002; Moureau et al., 2004) with the inclusion of chemical source terms (Sutherland and Kennedy, 2003).

5 Numerical issues

5.1 Effective wave number

In many cases, turbulence results from the development, amplification and saturation of unstable hydrodynamic modes of the main flow. Thus, any numerical method used to compute such flow must be able to represent the growth of these modes, viz. it must not be too dissipative. Besides, since the scale separation can be large in high-Reynolds number flows (the integral to Kolmogorov length scale ratio behaves like $R^{3/4}$, with $R = k^2/(\nu\epsilon)$, where k is the turbulent kinetic energy, ν the cinematic viscosity and ϵ the rate of energy dissipation), it is worth minimizing the number of grid point necessary to represent the smallest scales. Moreover, the effective dissipation at the Kolmogorov scale level must not be overestimated if the actual Reynolds number of the flow is to be accounted for (with $R = k^2/(\nu\epsilon)$, any extra dissipation decreases R). Thus an important constraint put on the numerics is that the numerical dissipation is as small as possible for all the length scales present in the flow. This is the reason why spectral methods have been considered, till the early 90's, as the only appropriate methods for performing direct or large-eddy simulations of turbulent flows.

These methods have been introduced by Orszag (1969). Their main interest is that there is no dispersion/dissipation error associated to the estimation of spatial derivatives until the cut-off wave number π/Δ is reached, with Δ the mesh size. A Fourier decomposition is used most often in homogeneous directions while Chebishev polynoms are preferred when periodicity cannot be assumed. The main drawback of fully spectral methods is related to the non-linear term (convection) of the Navier-Stokes equations. Compute these terms in the frequency space requires assessing convolution products by triadic summation, a rather CPU consuming process. This has motivated the development of pseudo-spectral methods where only the diffusive and pressure terms are computed in the frequency space, the physical space being used for assessing the convective contribution. Of course this approach requires a fast and accurate way to pass from one space to the other since such transformation is done twice per iteration. Note that spectral methods are not exact, even if there is no error in the assessment of the spatial derivatives. The aliasing error is related to the non-linear terms and from scales which cannot be represented on the computational grid. Such scale can potentially appear when two small (but resolved) scales are multiplied together (simply because $\cos \alpha \sin \alpha \propto \sin 2\alpha$). In spectral methods, these errors are usually avoided thanks to the 2/3 rule which consists in using information from only a part of the Fourier modes that can be represented on the computational grid. In spite of this limitation, spectral methods are certainly the method of choice for performing large-eddy or direct simulations of simple configurations (e.g. incompressible flow, with 2 or 3 homogeneous directions). However, despite some work about spectral elements (Orszag and Patera, 1984; Henderson and Kardianakis, 1995; Chu and Karniadakis, 1993), spectral methods are not well suited to complex geometries. More details about spectral methods can be found in Canuto et al. (1988).

In the case of complex geometries or boundary conditions, spectral methods cannot be used and the simulations must be based on either a finite volume, a finite element or a finite difference method. In the finite volume method, volume integrals of the conservative equations are taken over each cell of the mesh and converted to surface integrals, using

the divergence theorem. These terms are then evaluated as fluxes at the faces of each finite volume. Because the flux entering a given volume is identical to that leaving the adjacent volume, these methods are conservative in nature. In the finite element method, the flow motion equation are first written in the weak form. The best approximation of the corresponding solution is then sought for in the linear space spanned by a set of basis functions related to the computational mesh. Finding this best approximation amounts to determining its components in the basis function, viz. solving a set of ordinary differential equations. The order of accuracy of the method can be made arbitrarily large (at least theoretically) by using higher order elements (e.g.: replacing piecewise linear elements by piecewise quadratic elements). Eventually, the finite difference method consists in approximating each partial derivatives of the flow equations by finite difference formula which are obtained by combining Taylor series of the nodal unknowns. This results in a system of algebraic equations whose unknown are the nodal values of the flow quantities (velocity, pressure, ...).

The three methods mentioned above can be used for performing unsteady simulation as long as appropriate spatial scheme and temporal time stepping procedure are used. The finite volume and finite elements methodologies are well suited to complex geometries since they can be formulated within an unstructured mesh framework. Finite differences are more intuitive but only appropriate to simple geometries since the computational grid must be cartesian. Note that in 1D, the three methods are equivalent so that the finite difference framework is often used for analysing numerical schemes.

As mentioned earlier in this section, the numerical error must be controlled and minimized for all the length scales present in the unsteady flow to be computed. This means that the accuracy of a numerical scheme cannot be only reduced to its order of accuracy. This is different from the case of the numerical methods devoted to steady flow computations for which higher order usually means higher overall accuracy. As far as unsteady flow computations are concerned, it is necessary to perform a wavelength based numerical analysis. In the spectral analysis, one considers an harmonic perturbation of the form $f(x) = \exp(jkx)$ and compares how the discrete and the exact derivatives operate on this perturbation. For example, consider the first spatial derivative and its second order centered approximation:

$$\frac{df}{dx}(x_i) \equiv \frac{f_{i+1} - f_{i-1}}{2\Delta x} \quad (83)$$

where Δx is the distance (supposed constant) between two consecutive nodes and f_i stands for $f(x_i)$. Injecting $f(x) = \exp(jkx)$ into equation 83 leads to:

$$\frac{df}{dx}(x_i) \equiv jk' \exp(jkx_i), \quad \text{with} \quad k' = \frac{\sin(k\Delta x)}{\Delta x} \quad (84)$$

where k' is the effective wavenumber of the perturbation once its derivative is assessed by the finite difference formula 83. The effective-to-exact wavenumber ratio can then be used to quantify the errors related to the numerical scheme. In the above example this ratio is:

$$\frac{k'}{k} = \frac{\sin(k\Delta x)}{k\Delta x} \quad (85)$$

Consider the simple linear convection equation:

$$\frac{\partial f}{\partial t} + u_0 \frac{\partial f}{\partial x} = 0 \quad (86)$$

From equation 84, solving equation 86 with perfect time integration and finite difference 83 is equivalent to solve exactly the following equation:

$$\frac{\partial f}{\partial t} + u_0 \frac{\sin(k\Delta x)}{k\Delta x} \frac{\partial f}{\partial x} = 0 \quad (87)$$

Thus the k'/k ratio can also be interpreted as the error in the speed of propagation of a perturbation of wavelength k . In the general case, the k'/k ratio can be written in the form $k'/k = E(k\Delta x) = E_r(k\Delta x) + jE_i(k\Delta x)$ and the effective equation is:

$$\frac{\partial f}{\partial t} + u_0 E(k\Delta x) \frac{\partial f}{\partial x} = 0 \quad (88)$$

Assuming that the initial condition is $f(x, t = 0) = \exp(jkx)$, the exact solution of equation 88, viz. the numerical solution of equation 86, is simply:

$$f(x, t > 0) = \exp(jk(x - E(k\Delta x)u_0t)) = \exp(kE_i(k\Delta x)u_0t) \exp(jk(x - E_r(k\Delta x)u_0t)) \quad (89)$$

When $k\Delta x$ tends to zero the number of grid point per wavelength tends to infinity, the $k'/k = E(k\Delta x)$ tends to unity and the exact solution of equation 86 is recovered, viz. $\exp(jk(x - u_0t))$. In the case where the imaginary part of k'/k is not zero, viz. $E_i(k\Delta x) \neq 0$, the amplitude of the harmonic perturbation is not conserved; it is damped if $E_i(k\Delta x) < 0$ and it becomes unbounded if $E_i(k\Delta x) > 0$. The effective-to-exact wavelength ratios relative to some classical finite difference schemes are reported in table 4 and plotted in figure 17.

The centered finite difference schemes have pure real k'/k ratio and thus are non dissipative, whatever their order is. This property is not shared by the biased schemes which all introduce an amount of dissipation. Comparing the analysis for the 2nd order centered and upwind schemes it is clear that the order of accuracy is not enough to qualify the properties of a scheme; the centered one is non dissipative whereas the second one dissipates energy. Actually one can show that the order of accuracy is related to the behavior of $E(k\Delta x)$ when $k\Delta x$ goes to zero, namely $E(k\Delta x) - 1 \propto (k\Delta x)^p$ if the scheme is of order p . Note also that a property shared by all the finite difference schemes is that they cannot propagate wiggles accurately ($E(\pi) = 0$).

As an illustration of the effect of the above described numerical errors, the results obtained for different schemes applied to equation 86 with $u_0 = 1$ m/s and $f(x, t = 0) = \exp(-x^2/4a^2)$ with $a = 0.2$ m are presented in figure 18. Three different resolutions are compared for the four schemes discussed above. The computational domain is taken wide

FD	name	E_r	E_i
$\frac{f_i - f_{i-1}}{\Delta x}$	1st order upwind	$\frac{\sin(k\Delta x)}{k\Delta x}$	$\frac{\cos(k\Delta x) - 1}{k\Delta x}$
$\frac{f_{i+1} - f_{i-1}}{2\Delta x}$	2nd order centered	$\frac{\sin(k\Delta x)}{k\Delta x}$	0
$\frac{3f_i - 4f_{i-1} + f_{i-2}}{2\Delta x}$	2nd order upwind	$\frac{\sin(k\Delta x)}{k\Delta x} (2 - \cos(k\Delta x))$	$\frac{-\cos(2k\Delta x) + 4\cos(k\Delta x) - 3}{k\Delta x}$
$\frac{-f_{i+2} + 8f_{i+1} - 8f_{i-1} + f_{i-2}}{12\Delta x}$	4th order centered	$\frac{\sin(k\Delta x)}{3k\Delta x} (4 - \cos(k\Delta x))$	0

Table 4: Classical finite difference formula for the spatial first derivative and associated error.

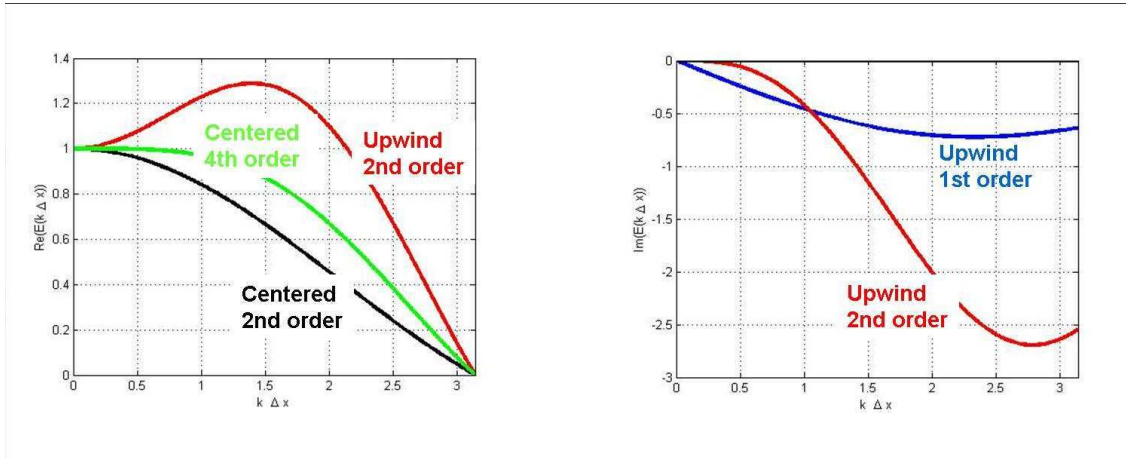


Figure 17: Effective-to-exact wavelength ratios for the schemes displayed in table 4. The imaginary part (right plot) is zero for centered schemes. The 1st order upwind and the 2nd order centered schemes share the same real part (left plot). These graphs can be interpreted as the effective-to-exact convection velocity ratio, or as the effective-to-exact first derivative ratio.

enough to avoid spurious boundary effects; the time step has been chosen small enough to consider that the numerical errors are only related to the spatial discretization. The dissipative nature of the upwind schemes appear clearly in this figure (first row) which also demonstrate that two schemes with the same order of accuracy can lead to very different unsteady results (compare the 2nd and 3rd rows). Note that the decrease of signal amplitude observed for the 2nd order centered scheme should not be associated to a dissipation of energy; it is actually a dispersive effect, viz. the different Fourier modes which constitute the initial Gaussian perturbation are not convected at the same velocity because the k'/k ratio depends on $k\Delta x$. For this scheme, this ratio is less than unity (see figure 17) and the signal tends to be delayed (see figure 18, second row). On the contrary, the real part of the k'/k ratio is greater than unity for the 2nd order upwind scheme (see figure 17) and consistently the computed pulse tends to be in advance at time $t=5$ s (see figure 18, third row). Note that the 1st order upwind scheme suffers from the same dispersive error than the 2nd order scheme (they have the same real part of k'/k); however, the dissipative error for this scheme is so large that the signal distortion is not apparent in the first row of figure 18.

The same kind of analysis can be done for analysing second derivative formula. The k'^2/k^2 ratios corresponding to two different 2nd order centered schemes are displayed in figure 19. The two schemes considered are the 3-point stencil scheme:

$$\frac{d^2 f}{dx^2}(x_i) \equiv \frac{f_{i+1} - 2f_i + f_{i-1}}{\Delta x^2} \quad (90)$$

and the 5-point stencil scheme:

$$\frac{d^2 f}{dx^2}(x_i) \equiv \frac{f_{i+2} - 2f_i + f_{i-2}}{4\Delta x^2} \quad (91)$$

The first scheme can be obtained from Taylor series written at node i . The latter one is obtained by two successive applications of the 2nd order centered scheme 83 for the

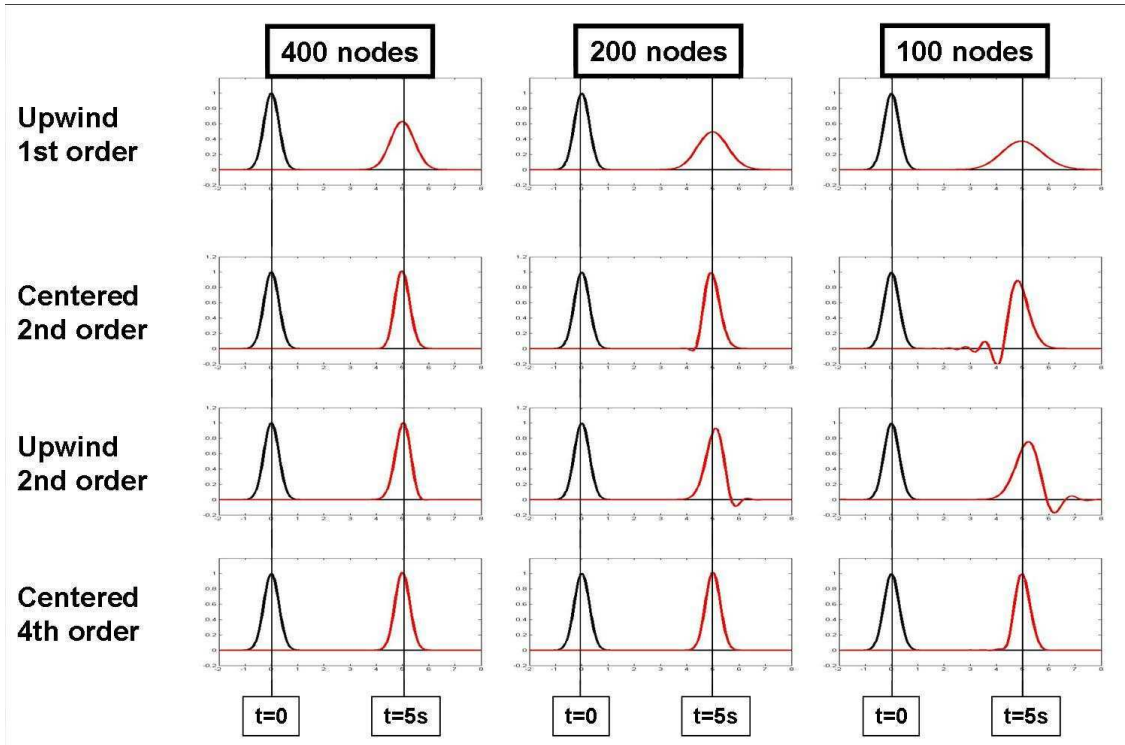


Figure 18: Numerical convection of a Gaussian pulse with the finite difference schemes presented in table 4. The vertical line indicates the theoretical position of the maximum of the Gaussian perturbation.

first derivative. This way of discretizing second derivatives is often chosen in 3D codes for complex geometries because of its simplicity. Although both second order accurate, these two schemes have different spectral responses, as illustrated in figure 19. The limiting behaviors when $k\Delta x \rightarrow 0$ are of course the same since these schemes share the same order of accuracy. However, when $k\Delta x \rightarrow \pi$ the 3-point stencil scheme is much more accurate than the 5-point scheme. For the latter one, the effective diffusion coefficient tends to zero near the cut-off wavenumber. It is important to note that such a numerical behavior is not acceptable for LES of turbulent flows (Nicoud et al., 1998). Indeed, the effective energy dissipation at the small scales is always close to zero, whatever the SGS model is. As a result, the energy flux from the largest to the smallest scales cannot be balanced and there is an energy accumulation at the smallest resolved scales. This behavior is illustrated in figure 20.

5.2 Handling stability issues

A key issue when performing LES of turbulent flows is the necessity to use virtually non-dissipative schemes to handle flow fields which contain a lot of energy at large wave numbers. Since numerical errors are large for the smallest scales, the risk for such computation to run unstable is real. Thus some kind of stabilization technique must be used, especially when the LES is performed on a complex geometry. Different approaches can be used, depending on the nature of the equation solved. Note that the stability issues that are dealt with in this section are related to the non-linearity of the flow equations. In

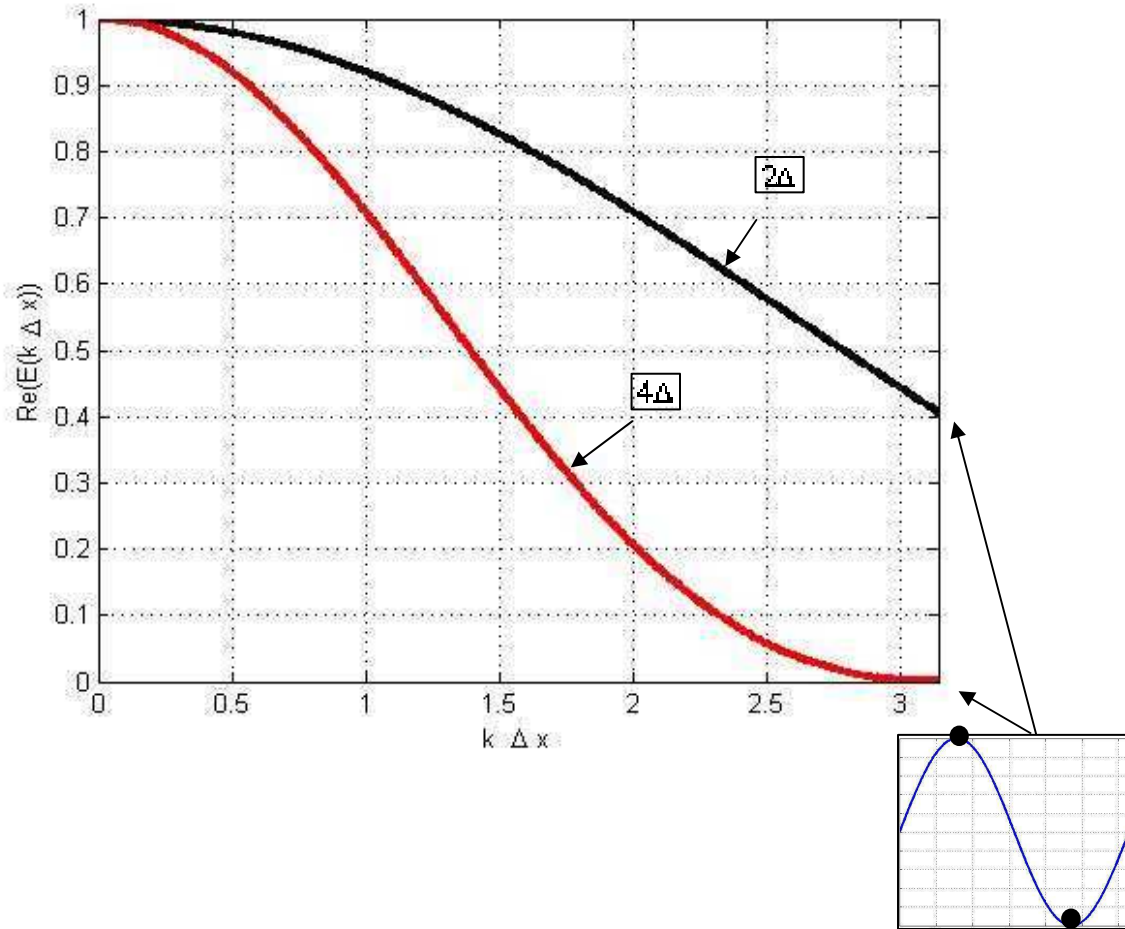


Figure 19: Effective-to-exact wavelength ratios for the 3-point and 5-point stencil (real part). These graphs can be interpreted as the effective-to-exact diffusion coefficient ratio, or as the effective-to-exact second derivative ratio.

other words, we are talking about instabilities arising from simulations based on *linearly stable* schemes. As such, these issues are out of reach of a classical stability analysis (for example the Von Neumann analysis).

5.2.1 Kinetic energy conservation

As far as incompressible Navier-Stokes equations are concerned, experience has shown that the kinetic energy must be conserved if a stable and dissipation-free numerical method is sought. Indeed, such property ensures that the sum of the square of the velocities cannot grow, even through non-linear interactions between modes. As a consequence, a numerical scheme which conserves kinetic energy cannot be unstable. Moreover, it makes unnecessary the use of numerical stabilization through up-winding which is known to introduce too much artificial damping in DNS/LES computations. Morinishi et al. (1998) developed a set of fully conservative (mass, momentum and kinetic energy) high order schemes for incompressible flow. A formulation adapted to cylindrical coordinates was proposed by Morinishi et al. (2004) and a generalization to low-Mach number flows was proposed by Nicoud (2000). A key ingredient in such approach is the use of a skew-

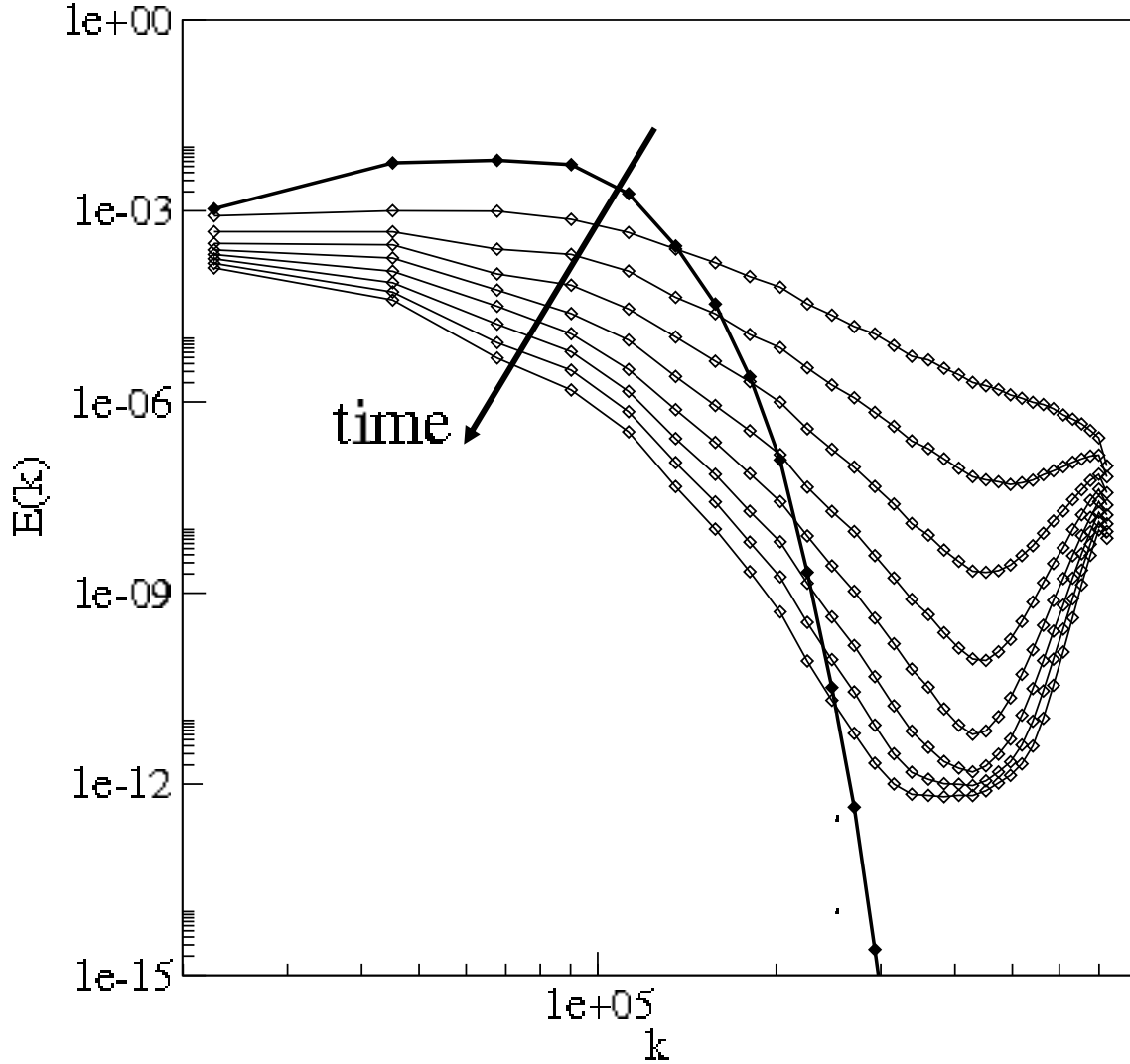


Figure 20: Time evolution of the turbulent kinetic energy spectrum from a LES of homogeneous isotropic turbulence performed with a 5-point stencil scheme for the diffusive terms.

symmetric form of the non-linear term. This latter reads:

$$\text{Convection} = \frac{1}{2} u_j \frac{\partial u_i}{\partial x_j} + \frac{1}{2} \frac{\partial u_i u_j}{\partial x_j} \quad (92)$$

and is neither equal, in the discrete sense, to the divergence ($\partial u_i u_j / \partial x_j$) nor the convective ($u_j \partial u_i / \partial x_j$) form, even if, the flow being incompressible, the velocity divergence is zero ($\partial u_j / \partial x_j = 0$). Discuss the details of such kinetic energy conserving scheme for the low-Mach number or incompressible Navier-Stokes equations is out of the scope of this course. All the details can be found in the references cited above; see also Mahesh et al. (2004) for a second order accurate implementation appropriate for unstructured meshes. To give a flavor of the importance of the form used to represent the non-linear term, the case of the 1D Burgers equation is discussed in the following. One considers solving

$$\frac{\partial u}{\partial t} + \frac{\partial u^2}{\partial x} = 0 \quad (93)$$

over a 1D periodic domain $0 < x < L$. Multiplying equation 93 by u and integrating over space, the overall kinetic energy $K = \int_{x=0}^L u^2 dx / 2$ follows the following equation:

$$\frac{dK}{dt} = - \int_{x=0}^L u \frac{\partial u^2}{\partial x} dx \quad (94)$$

The RHS can be readily integrated as follows:

$$\int_{x=0}^L u \frac{\partial u^2}{\partial x} dx = 2 \int_{x=0}^L u^2 \frac{\partial u}{\partial x} dx = 2 \left[\frac{u^3}{3} \right]_0^L \quad (95)$$

which is zero since L-periodicity is assumed. Thus the overall kinetic energy should be conserved, whatever the initial condition is.

Suppose a random periodic field is used to initialize the computation over a uniform mesh. Suppose also that no significant error is introduced by the time integration. The numerical test consists in computing a few turn over times $L/\sqrt{K(t=0)}$ and check whether a) the computation is stable and b) K remains constant. Several spatial schemes have

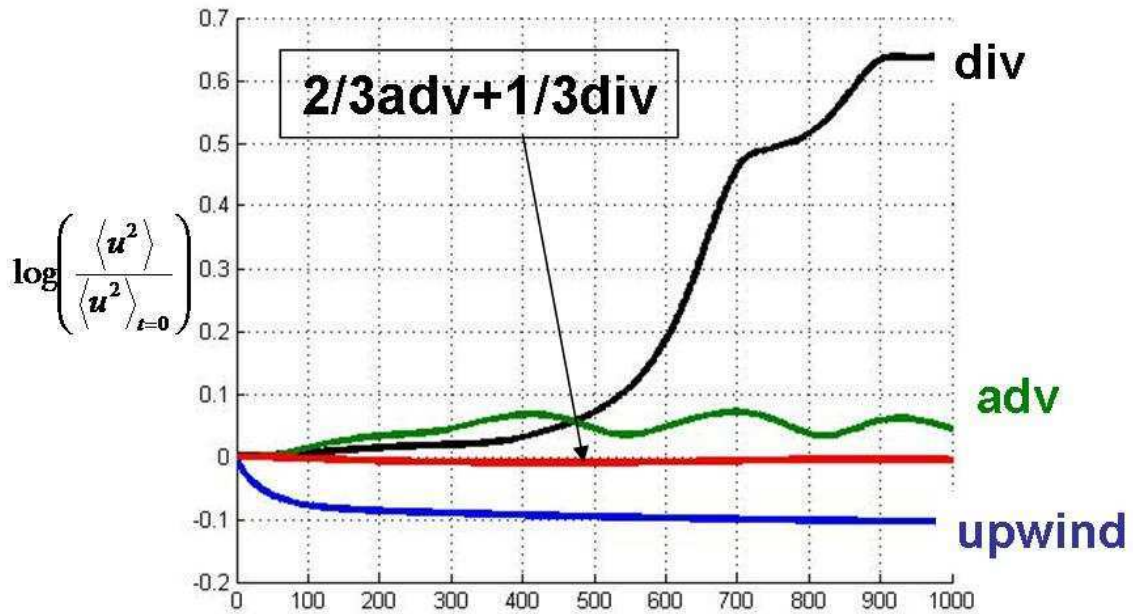


Figure 21: Time evolution of the overall kinetic energy from the Burgers equation in the L-periodic domain. Only the mixed scheme of equation 98 lead to the expected constant evolution.

tested (see table 5) and the results are plotted in figure 21. As expected, the 1st order upwind leads to a stable computation but introduces a significant energy dissipation. With the centered schemes based on the divergence and the advective forms, the kinetic energy tends to increase over time, especially with the divergence form which proved unstable in many cases. These formulations are indeed not conservative for the kinetic energy, as it is apparant when multiplying the non-linear term at node i by the nodal velocity value u_i at the same place and summing all the contributions. For the divergence form one

name	form of the convective term	FD scheme
upwind	$\frac{\partial u^2}{\partial x}$	$\frac{u_i^2 - u_{i-1}^2}{\Delta x}$
advective	$2u \frac{\partial u}{\partial x}$	$2u_i \frac{u_{i+1} - u_{i-1}}{2\Delta x}$
divergence	$\frac{\partial u^2}{\partial x}$	$\frac{u_{i+1}^2 - u_{i-1}^2}{2\Delta x}$
mixed	$\frac{4}{3}u \frac{\partial u}{\partial x} + \frac{1}{3} \frac{\partial u^2}{\partial x}$	$4u_i \frac{u_{i+1} - u_{i-1}}{6\Delta x} + \frac{u_{i+1}^2 - u_{i-1}^2}{6\Delta x}$

Table 5: Finite difference schemes tested for solving the Burgers equation 93.

obtains:

$$\begin{array}{rcl}
 \text{Node } i - 2 : & & \dots \\
 \text{Node } i - 1 : & & u_{i-1} \frac{u_i^2 - u_{i-2}^2}{2\Delta x} \\
 \text{Node } i : & & u_i \frac{u_{i+1}^2 - u_{i-1}^2}{2\Delta x} \\
 \text{Node } i + 1 : & & u_{i+1} \frac{u_{i+2}^2 - u_i^2}{2\Delta x} \\
 \text{Node } i + 2 : & & \dots \\
 \hline
 2\Delta x \times \text{Sum} : & \dots + \underbrace{u_{i-1}u_i^2 - u_i u_{i-1}^2}_{\dots} + \underbrace{u_i u_{i+1}^2 - u_{i+1} u_i^2}_{\dots} + \dots & (96)
 \end{array}$$

whereas for the advective form:

$$\begin{array}{rcl}
 \text{Node } i - 2 : & & \dots \\
 \text{Node } i - 1 : & & 2u_{i-1}^2 \frac{u_i - u_{i-2}}{2\Delta x} \\
 \text{Node } i : & & 2u_i^2 \frac{u_{i+1} - u_{i-1}}{2\Delta x} \\
 \text{Node } i + 1 : & & 2u_{i+1}^2 \frac{u_{i+2} - u_i}{2\Delta x} \\
 \text{Node } i + 2 : & & \dots \\
 \hline
 \Delta x \times \text{Sum} : & \dots + \underbrace{u_{i-1}^2 u_i - u_i^2 u_{i-1}}_{\dots} + \underbrace{u_i^2 u_{i+1} - u_{i+1}^2 u_i}_{\dots} + \dots & (97)
 \end{array}$$

Note that the errors in the kinetic energy associated to the divergence and advective schemes have similar forms and it is thus possible to combine these two discretizations to generate a kinetic energy conserving scheme. Namely, comparing equations 96 and 97, it is clear that the following scheme:

$$\frac{2}{3}adv + \frac{1}{3}div = 4u_i \frac{u_{i+1} - u_{i-1}}{6\Delta x} + \frac{u_{i+1}^2 - u_{i-1}^2}{6\Delta x} \quad (98)$$

should be conservative. This result is nicely supported by the numerical result of figure 21.

It should be noted that the concept of kinetic energy conservation is only valid for incompressible or low-Mach number flows. Since there is no extension of this principle to compressible situations, one should rely on numerical stabilization via artificial viscosity to stabilize LES of such flow.

5.2.2 Artificial viscosity

In order to minimize numerical dissipation, the spatial schemes used for LES are often essentially centered. An example of such scheme is provided in Colin and Rudgyard (2000)

(see also Moureau et al. (2005) for its extension to moving grids). These authors developed a Taylor Galerkin scheme (Donea et al., 1987) suitable for LES over unstructured meshes and third order accurate in both time and space. An interesting feature of this scheme is that, besides being essentially non-dissipative, its dispersion error was minimized by tuning the free parameters of the general two-steps method.

When a non-dissipative scheme is used, the (unavoidable) numerical perturbations generated throughout the computational domain are not damped efficiently, especially when high Reynolds number flows are considered. When the flow domain is unbounded (as in external aerodynamics for example), one can deal with this issue, at least partly, by using non-reflecting boundary conditions which let the unphysical perturbations leave the domain. Regarding wall bounded flows (as in combustors for example), the situation is more critical since the unphysical perturbations can neither be damped nor evacuated through boundaries. This is why it is common practice to add a so-called artificial viscosity (AV) term to the discrete equations, to avoid spurious oscillations (also known as “wiggles”) and in order to smooth very strong gradients. We describe here different methods which can be used and which proved useful in practical applications.

These AV models are characterized by the ‘linear preserving’ property which leaves unmodified a linear solution on any type of element. The models are based on a combination of a “shock capturing” term (called 2nd order AV) and a “background dissipation” term (called 4th order AV). Adding AV in a code is done in two steps:

- first a sensor detects if AV is necessary, as a function of the flow characteristics,
- then a certain amount of 2nd and 4th AV is applied, depending on the sensor value and on user-defined parameters.

Classical Sensors:

A sensor ζ_{Ω_j} is a scaled parameter which is defined for every cell Ω_j of the domain and which takes values from zero to one; $\zeta_{\Omega_j} = 0$ means that the solution is well resolved and that no AV should be applied while $\zeta_{\Omega_j} = 1$ signifies that the solution has strong local variations and that AV must be applied. This sensor is obtained by comparing different evaluations (on different stencils) of the gradient of a given scalar (pressure, total energy, mass fractions, ...). If these gradients are identical, then the solution is locally linear and the sensor is zero. On the contrary, if these two estimations are different, local non-linearities are present, and the sensor is activated. The key point is to find a suitable sensor-function that is non-zero only at places where stability problems occur. A widely used sensor is the one proposed by Jameson et al. (1981).

For every cell Ω_j , the Jameson cell-sensor $\zeta_{\Omega_j}^J$ is the maximum over all cell vertices of the Jameson vertex-sensor ζ_k^J :

$$\zeta_{\Omega_j}^J = \max_{k \in \Omega_j} \zeta_k^J \quad (99)$$

Denoting S the scalar quantity the sensor is based on (usually S is the pressure), the Jameson vertex-sensor is:

$$\zeta_k^J = \frac{|\Delta_1^k - \Delta_2^k|}{|\Delta_1^k| + |\Delta_2^k| + |S_k|} \quad (100)$$

Where the Δ_1^k and Δ_2^k functions are defined as:

$$\Delta_1^k = S_{\Omega_j} - S_k \quad \Delta_2^k = (\vec{\nabla}S)_k \cdot (\vec{x}_{\Omega_j} - \vec{x}_k) \quad (101)$$

where the k subscript denotes cell-vertex values while Ω_j is the subscript for cell-averaged values. $(\vec{\nabla}S)_k$ is the gradient of S at node k . Δ_1^k measures the variation of S inside the cell Ω_j (using only quantities defined on this cell). Δ_2^k is an estimation of the same variation but on a wider stencil (using all the neighboring cell of the node k).

For example, on a 1D uniform mesh, of mesh size Δx and for the cell $[k\Delta x; (k+1)\Delta x]$, the Δ_1^k and Δ_2^k functions are estimated as follows:

$$\Delta_1^k = \frac{\Delta x}{2} \frac{S_{k+1} - S_k}{\Delta x} \quad \Delta_2^k = \frac{\Delta x}{2} \frac{S_{k+1} - S_{k-1}}{2\Delta x} \quad (102)$$

The numerator of eq. (100) is then

$$|\Delta_1^k - \Delta_2^k| = \frac{\Delta x^2}{4} \left| \frac{S_{k+1} - 2S_k + S_{k-1}}{\Delta x^2} \right| = \frac{\Delta x^2}{4} |\Delta_{k,\Delta x}^{FD} S| \quad (103)$$

$\Delta_{k,\Delta x}^{FD}$ is exactly the classical FD Laplacian operator evaluated at vertex k and of size Δx . The Jameson sensor is thus proportional to the second derivative of S , which is zero when S is linear and which is maximum when the gradient of S varies rapidly. This is what happens for example on each side of a front or when wiggles occur.

The Jameson sensor is smooth and was initially derived for steady-state computations: it is roughly proportional to the amplitude of the deviation from linearity. For most unsteady turbulent computations it is however necessary to have a sharper sensor, which is very small when the flow is sufficiently resolved, and which is nearly maximum when a certain level of non-linearities occurs. Useful properties for a sensor $\zeta_{\Omega_j}^C$ adapted to unsteady calculations can be summarized as follows:

- $\zeta_{\Omega_j}^C$ is very small when both Δ_1^k and Δ_2^k are small compared to S_{Ω_j} . This corresponds to low amplitude numerical errors (when Δ_1^k and Δ_2^k have opposite signs) or smooth gradients that are well resolved by the scheme (when Δ_1^k and Δ_2^k have the same sign).
- $\zeta_{\Omega_j}^C$ is small when Δ_1^k and Δ_2^k have the same sign and the same order of magnitude, even if they are quite large. This corresponds to stiff gradients well resolved by the scheme.
- $\zeta_{\Omega_j}^C$ is big when Δ_1^k and Δ_2^k have opposite signs and one of the two term is large compared to the other. This corresponds to a high-amplitude numerical oscillation.
- $\zeta_{\Omega_j}^C$ is big when either Δ_1^k or Δ_2^k is of the same order of magnitude as S_{Ω_j} . This corresponds to a non-physical situation that originates from a numerical problem.

The following sensor (proposed by O. Colin during his PhD work at CERFACS) meets the above mentioned properties:

$$\zeta_{\Omega_j}^C = \frac{1}{2} \left(1 + \tanh \left(\frac{\Psi - \Psi_0}{\delta} \right) \right) - \frac{1}{2} \left(1 + \tanh \left(\frac{-\Psi_0}{\delta} \right) \right) \quad (104)$$

with:

$$\Psi = \max_{k \in \Omega_j} \left(0, \frac{\Delta^k}{|\Delta^k| + \epsilon_1 S_k} \zeta_k^J \right) \quad (105)$$

$$\Delta^k = |\Delta_1^k - \Delta_2^k| - \epsilon^k \max(|\Delta_1^k|, |\Delta_2^k|) \quad (106)$$

$$\epsilon^k = \epsilon_2 \left(1 - \epsilon_3 \frac{\max(|\Delta_1^k|, |\Delta_2^k|)}{|\Delta_1^k| + |\Delta_2^k| + S_k} \right) \quad (107)$$

Possible numerical values are:

$$\Psi_0 = 2.10^{-2} \quad \delta = 1.10^{-2} \quad \epsilon_1 = 1.10^{-2} \quad \epsilon_2 = 0.95 \quad \epsilon_3 = 0.5 \quad (108)$$

Artificial viscosity model:

Artificial viscosity can be used in many different ways in a CFD code. The term “model” denotes a combination of several parameters:

- the choice of the sensor and the variable which is used for the sensor,
- the way the 2nd order and the 4th order operators are combined,
- and finally on which variables the operators are applied.

A classical implementation uses the ‘Jameson’ sensor, equation 99, applied to the static pressure.

$$\zeta^{JAM} = \zeta_{\Omega_j}^J(P) \quad (109)$$

The amount of 2nd order AV that is applied is directly proportional to this sensor and to the user parameter `smu2`. The amount of 4th order AV also depends on the sensor. Actually, the input parameter `smu4` is replaced by:

$$\text{smu4}' = \max(0, \text{smu4} - \zeta^{JAM} \text{smu2}) \quad (110)$$

This formulation allows to put 4th order AV only where the sensor is small (as well as the amount of 2nd order AV). On the other hand, if the sensor is large, it is no use to put 4th order AV, because the 2nd order AV operates fully and overcomes most of the problems. Both operators are applied on all variables (momentum, energy and species).

This model was originally proposed by Jameson et al. (1981). It is very well suited for “aerodynamics” configurations, with shocks and without combustion, solved with a RANS solver. However it appears that for reacting LES, this model is much too dissipative and must only be used during transient phases. It allows to stabilize a computation when non-physical processes of high amplitudes happen (at the initialization phase for example). An AV implementation based on the Colin sensor described above, equation 104 proved more suitable for unsteady calculations. Moreover, the experience shows that it is often useful to apply the 4th order AV term only to the mass and energy equations. In doing so, no artificial damping is added to the momentum equation and a significant part of the resolved kinetic energy can be affected to the smallest scales, as it is expected in LES. More details about this implementation can be found in Colin (2000).

References

- Anderson, J. (1982). Modern compressible flow (with historical perspective). *McGraw-Hill, New-York*.
- Atkins, H. and Casper, J. (1994). Nonreflective boundary conditions for high-order methods. 32(3):512–518.
- Baum, M., Poinso, T. J., and Thévenin, D. (1994). Accurate boundary conditions for multicomponent reactive flows. *Journal of Computational Physics*, 116:247–261.
- Bird, R., Stewart, W., and Lightfoot, E. (1960). *Transport Phenomena*. John Wiley & Sons, New York.
- Buell, J. and Huerre, P. (1988). Inflow/outflow boundary conditions and global dynamics of spatial mixing layers. *Center for Turbulence Research, CTR Annual Research Briefs*, pages 19–27.
- Canuto, C., Hussaini, M., Quarteroni, A., and Zang, T. (Springer Verlag, 1988). Spectral methods in fluid dynamics. *Springer Series in Computational Physics*.
- Chakravarthy, S. (1983). Euler equations - implicit scheme and boundary condition. 21:699–706.
- Chassaing, P. (2000). *Turbulence en mécanique des fluides, analyse du phénomène en vue de sa modélisation à l'usage de l'ingénieur*. Cépaduès-éditions, Toulouse, France.
- Chu, D. and Karniadakis, G. (1993). A direct numerical simulation of laminar and turbulent flow over riblet-mounted surfaces. 250:1–42.
- Colin, O. (2000). *Simulations aux grandes échelles de la combustion turbulente prémélangée dans les statoréacteurs*. PhD thesis, INP Toulouse.
- Colin, O. and Rudgyard, M. (2000). Development of high-order Taylor-Galerkin schemes for unsteady calculations. *Journal of Computational Physics*, 162(2):338–371.
- Colonus, T., Lele, S., and Moin, P. (1993). Boundary conditions for direct computation of aerodynamic sound generation. 31(9):1574–1582.
- Comte, P., Ducros, F., Silvestrini, J., David, E., Lamballais, E., Métais, O., and Lesieur, M. (1994). Simulation des grandes échelles d'écoulements transitionnels. *AGARD Conference proceedings 551*, pages 14–1/14–11.
- Donea, J., Quartapelle, L., and Selmin, V. (1987). An analysis of time discretization in the finite element solution of hyperbolic problems. *Journal of Computational Physics*, 70:463–499.
- Ducros, F., Comte, P., and Lesieur, M. (1996). Large-eddy simulation of transition to turbulence in a boundary layer spatially developing over a flat plate. *J. Fluid Mech.*, 326:1–36.

- Engquist, B. and Majda, A. (1977). Absorbing boundary conditions for the numerical simulation of waves. *Mathematics of Computation*, 31(139):629–651.
- Freund, J. (1997). Proposed inflow/outflow boundary condition for direct computation of aerodynamic sound. 35(4):740–742.
- Germano, M., Piomelli, U., Moin, P., and Cabot, W. (1991). A dynamic subgrid-scale eddy viscosity model. *Physics of Fluids*, 3(7):1760–1765.
- Ghosal, G., Lund, T., Moin, P., and Akselvoll, K. (1995). A dynamic localization model for large-eddy simulation of turbulent flows. *J. Fluid Mech.*, 286:229–255.
- Giles, M. (1990). Non-reflecting boundary conditions for euler equation calculation. 28(12):2050–2058.
- Givoli, D. (1991). Non-reflecting boundary conditions. 94:1–29.
- Gottlieb, D. and Turkel, E. (1978). Boundary conditions for multistep finite difference methods for time-dependent equations. 26:181–196.
- Griffin, M. and Anderson, J. (1977). On the application of boundary conditions to time dependent computations for quasi-one dimensional fluid flows. *Computers and Fluids*, 5:127–137.
- Gustafsson, B. and Sundstrom, A. (1978). Incompletely parabolic problems in fluid dynamics. *SIAM J. Appl. Math*, 35(2):343.
- Haselbacher, A. and Vasilyev, O. (2003). Commutative discrete filtering on unstructured grids based on least-squares techniques. *Journal of Computational Physics*, 187:197–211.
- Hayder, M. and Turkel, E. (1993). High order accurate solutions of viscous problems. *AIAA Paper 93-3074*.
- Hayder, M. and Turkel, E. (1995). Nonreflecting boundary conditions for jet flow computations. 33(12):2264–2270.
- Henderson, R. and Kardianakis, G. (1995). Unstructured spectral element methods for simulation of turbulent flows. 122(2):191–217.
- Higdon, R. (1986). Initial-boundary value problems for linear hyperbolic systems. *SIAM Rev.*, 28:177–217.
- Hirschfelder, J., Curtiss, C., and Bird, R. (1954). *Molecular Theory of Gases and Liquids*. John Wiley & Sons, New York.
- Hirsh, C. (1990). *Numerical computation of internal and external flow.*, volume 2. J. Wiley and Sons, New York.
- Jameson, A., Schmidt, W., and Turkel, E. (1981). Numerical solutions of the euler equations by finite volume methods using runge-kutta time-stepping schemes. AIAA paper 81-1259.

- Jansen, K. (1994). Unstructured-grid large-eddy simulation of flow over an airfoil. *Center for Turbulence Research, Annual Research Briefs*, pages 161–173.
- Kreiss, H. (1970). Initial boundary value problems for hyperbolic systems. *Commun. Pure Appl. Math.*, 23:277.
- Lesieur, M. and Métais, O. (1996). New trends in large-eddy simulations of turbulence. *Annual Rev. Fluid Mech.*, 28:45–82.
- Lilly, D. (1992). A proposed modification of the germano subgrid-scale closure method. *Phys. Fluids*, A4(3):633–635.
- Lund, T. and Novikov, E. (1992). Parameterization of subgrid-scale stress by the velocity gradient tensor. *Center for Turbulence Research, Annual Research Briefs*, pages 27–43.
- Mahesh, K., Constantinescu, G., and Moin, P. (2004). A numerical method for large-eddy simulation in complex geometries. *Journal of Computational Physics*, 197(1):215–240.
- Marsden, A., Vasilyev, O., and Moin, P. (2002). Construction of commutative filters for les on unstructured meshes. *Journal of Computational Physics*, 175:584–603.
- Mazaheri, K. and Roe, P. (1997). Numerical wave propagation and steady-state solutions: Soft wall and outer boundary conditions. 35(6):965–975.
- Mendez, S. and Nicoud, F. (2008). Large-eddy simulation of a bi-periodic turbulent flow with effusion. *Journal of Fluid Mechanics*, in press. MB.
- Meneveau, C., Lund, T., and Cabot, W. (1996). A lagrangian dynamic subgrid-scale model of turbulence. *Journal of Fluid Mechanics*, 319:353.
- Métais, O. and Lesieur, M. (1992). Spectral large-eddy simulation of isotropic and stably stratified turbulence. *J. Fluid Mech.*, 239:157–194.
- Moin, P. and Kim, J. (1982). Numerical investigation of turbulent channel flow. *J. Fluid Mech.*, 118:341.
- Moin, P. and Mahesh, K. (1998). Dns: a tool in turbulence research. *Annual Review in Fluid Mechanics*, 30:539–578.
- Morinishi, Y., Lund, T., Vasilyev, O., and Moin, P. (1998). Fully conservative higher order finite difference schemes for incompressible flow. *Journal of Computational Physics*, 143:90:124.
- Morinishi, Y., Vasilyev, O., and Ogi, T. (2004). Fully conservative finite difference scheme in cylindrical coordinates for incompressible flow simulations. *Journal of Computational Physics*, 197:686:710.
- Moureau, V., Lartigue, G., Sommerer, Y., Angelberger, C., Colin, O., and Poinso, T. (2004). Numerical methods for unsteady compressible multi-component reacting flows on fixed and moving grids. *Journal of Computational Physics*, 202(2):710–736.

- Moureau, V., Lartigue, G., Sommerer, Y., Angelberger, C., Colin, O., and Poinso, T. (2005). High-order methods for dns and les of compressible multi-component reacting flows on fixed and moving grids. *Journal of Computational Physics*, 202(2):710–736.
- Nicoud, F. (2000). Conservative high-order finite difference schemes for low-mach number flows. *Journal of Computational Physics*, 158:71–97.
- Nicoud, F. and Ducros, F. (1999). Subgrid-scale stress modelling based on the square of the velocity gradient tensor. *Flow, Turbulence and Combustion*, 62(3):183–200.
- Nicoud, F., Ducros, F., and Schönfeld, T. (1998). Towards direct and large eddy simulations of compressible flows in complex geometries. In *Notes in Numerical Fluid Mechanics*, pages 157–171. NF.
- Nicoud, F. and Schönfeld, T. (2002). Integral boundary conditions for unsteady biomedical cfd applications. *International Journal of Numerical Methods in Fluids*, 40:457–465.
- Okong’o, N. and Bellan, J. (2002). Consistent boundary conditions for multicomponent real gas mixtures based on characteristic waves. *Journal of Computational Physics*, 176:330–344.
- Orszag, S. (1969). Numerical methods for the simulation of turbulence. *Phys. Fluids*.
- Orszag, S. and Patera, A. (1984). A spectral element method for fluid dynamics; laminar flow in a channel expansion. 54.
- Poinso, T. and Lele, S. (1991). Boundary conditions for direct simulations of compressible viscous flows. 101:104–129.
- Poinso, T. and Veynante, D. (2001). Theoretical and numerical combustion. *R.T. Edwards Ed.*, page 473 pp.
- Polifke, W., Wall, C., and Moin, P. (2006). Partially reflecting and non-reflecting boundary conditions for simulation of compressible viscous flow. *Journal of Computational Physics*, 213:437–449.
- Pope, S. B. (2002). *Turbulent Flows*. Cambridge University Press, Cambridge UK.
- Prosser, R. (2005). Improved boundary conditions for the direct numerical simulation of turbulent subsonic flows i: Inviscid flows. *Journal of Computational Physics*, 207:736–768.
- Rockwell, D. and Naudascher, E. (1979). Self-sustained oscillations of impinging free shear layers. *Ann. Rev. Fluid Mech.*, 11:67–94.
- Rudy, D. H. and Strikwerda, J. C. (1980). A non-reflecting outflow boundary condition for subsonic navier stokes calculations. *Journal of Computational Physics*, 36:55–70.
- Sagaut, P. (1998). *Large Eddy Simulations for Incompressible Flows, An Introduction*. Springer-Verlag, New-York.

- Schmitt, P., Poinso, T., Schuermans, B., and Geigle, K. (2007). Large-eddy simulation and experimental study of heat transfer, nitric oxide emissions and combustion instability in a swirled turbulent high pressure burner. *Journal of Fluid Mechanics*, 570:17–46.
- Selle, L., Nicoud, F., and Poinso, T. (2004). The actual impedance of non-reflecting boundary conditions: implications for the computation of resonators. *AIAA Journal*, 42(5):958–964.
- Smagorinsky, J. (1963). General circulation experiments with the primitive equations, I. the basic experiment. *Monthly Weather Review*, 91(3):99–164.
- Stull, D. and Prophet, H. (1971). Janaf thermochemical tables, 2nd edition. Technical Report NSRDS-NBS 37, US National Bureau of Standards.
- Sutherland, J. and Kennedy, C. (2003). Improved boundary conditions for viscous, reacting, compressible flows. *Journal of Computational Physics*, 191:502–524.
- Ta’asan, S. and Nark, D. (1995). An absorbing buffer zone technique for acoustic wave propagation. *AIAA Paper 95-0146*.
- Tam, C. and Auriault, L. (1996). Time-domain impedance boundary conditions for computational aeroacoustics. 34(5):917–923.
- Thompson, K. (1987). Time dependant boundary conditions for hyperbolic systems. 68:1–24.
- Thompson, K. (1990). Time dependant boundary conditions for hyperbolic systems, ii. 89:439–461.
- Van Driest, E. (1956). On turbulent flow near a wall. *J. of Aero. Sci.*, 23:1007–1011.
- Vasilyev, O. V., Lund, T., and Moin, P. (1998). A general class of commutative filters for les in complex geometries. *Journal of Computational Physics*, 146:82–104.
- Vichnevetsky, R. and Bowles, J. (1982). Fourier analysis of numerical approximations of hyperbolic equations. *SIAM Philadelphia*.
- White, F. (1999). *Fluid Mechanics*. McGraw-Hill, 4th edition.
- Womersley, J. (1955). Method for the calculation of velocity, rate of flow and viscous drag in arteries when the pressure gradient is known. *Journal of Physiology*, 127:553–563.
- Wray, A. and Hunt, J. (1989). Algorithms for classification of turbulent structures. *Topological Fluid Mechanics, Proceedings of the IUTAM Symposium*, pages 95–104.
- Yee, H., Beam, R., and Warming, R. (1982). Boundary approximation for implicit schemes for one-dimensional inviscid equations of gas dynamics. 20:1203–1211.

A Governing equations for a multi-species, reacting gaseous mixture

Throughout the first part of this document, the index notation is adopted for the description of the governing equations. Summation rule is henceforth implied over repeated indices (Einstein's rule of summation). Note however that index k is reserved to refer to the k^{th} species and will not follow the summation rule unless specifically mentioned or implied by the \sum sign.

The set of conservation equation describing the evolution of a compressible flow with chemical reactions of thermodynamically active scalars reads,

$$\frac{\partial \rho u_i}{\partial t} + \frac{\partial}{\partial x_j}(\rho u_i u_j) = - \frac{\partial}{\partial x_j}[P \delta_{ij} - \tau_{ij}], \quad (111)$$

$$\frac{\partial \rho E}{\partial t} + \frac{\partial}{\partial x_j}(\rho E u_j) = - \frac{\partial}{\partial x_j}[u_i (P \delta_{ij} - \tau_{ij}) + q_j] + \dot{\omega}_T + Q_r, \quad (112)$$

$$\frac{\partial \rho_k}{\partial t} + \frac{\partial}{\partial x_j}(\rho_k u_j) = - \frac{\partial}{\partial x_j}[J_{j,k}] + \dot{\omega}_k. \quad (113)$$

In Eqs 111-113 respectively corresponding to the conservation laws for momentum, total energy and species, the following symbols denote respectively ρ , u_i , E , ρ_k , density, the velocity vector, the total energy per unit mass and $\rho_k = \rho Y_k$ for $k = 1$ to N (N is the total number of species). The source term in the total energy equation, Eq. 112s, is decomposed for convenience into a chemical source term and a radiative source term such that: $S = \dot{\omega}_T + Q_r$. Corresponding source terms in the species transport equations, Eq. 113, are noted, $\dot{\omega}_k$.

It is usual to decompose the flux tensor into an inviscid and a viscous component. They are respectively noted for the three conservation equations:

Inviscid terms:

$$\begin{pmatrix} \rho u_i u_j + P \delta_{ij} \\ (\rho E + P \delta_{ij}) u_j \\ \rho_k u_j \end{pmatrix} \quad (114)$$

where the hydrostatic pressure P is given by the equation of state for a perfect gas (Eq. 122).

Viscous terms:

The components of the viscous flux tensor take the form:

$$\begin{pmatrix} -\tau_{ij} \\ -(u_i \tau_{ij}) + q_j \\ J_{j,k} \end{pmatrix} \quad (115)$$

J_k is the diffusive flux of species k and is presented in section § A.3 (Eq. 133). The stress tensor τ_{ij} is explicated in section § A.4 (Eq. 134). Finally, section § A.5 is devoted to the heat flux vector q_j (Eq. 137).

A.1 Thermodynamical variables

The standard reference state we used is $P_0 = 1$ bar and $T_0 = 0$ K. The sensible mass enthalpies ($h_{s,k}$) and entropies (s_k) for each species are tabulated for 51 values of the temperature (T_i with $i = 1..51$) ranging from 0K to 5000K with a step of 100K. Therefore these variables can be evaluated by:

$$h_{s,k}(T_i) = \int_{T_0=0K}^{T_i} C_{p,k} dT = \frac{h_{s,k}^m(T_i) - h_{s,k}^m(T_0)}{W_k}, \quad \text{and} \quad (116)$$

$$s_k(T_i) = \frac{s_k^m(T_i) - s_k^m(T_0)}{W_k}, \quad \text{with } i = 1, 51 \quad (117)$$

The superscript m corresponds to molar values. The tabulated values for $h_{s,k}(T_i)$ and $s_k(T_i)$ can be found in the JANAF tables (Stull and Prophet, 1971). With this assumption, the sensible energy for each species can be reconstructed using the following expression :

$$e_{s,k}(T_i) = \int_{T_0=0K}^{T_i} C_{v,k} dT = h_{s,k}(T_i) - r_k T_i \quad i = 1, 51 \quad (118)$$

Note that the mass heat capacities at constant pressure $c_{p,k}$ and volume $c_{v,k}$ are supposed constant between T_i and $T_{i+1} = T_i + 100$. They are defined as the slope of the sensible enthalpy ($C_{p,k} = \frac{\partial h_{s,k}}{\partial T}$) and sensible energy ($C_{v,k} = \frac{\partial e_{s,k}}{\partial T}$). The sensible energy henceforth varies continuously with the temperature and is obtained by using a linear interpolation:

$$e_{s,k}(T) = e_{s,k}(T_i) + (T - T_i) \frac{e_{s,k}(T_{i+1}) - e_{s,k}(T_i)}{T_{i+1} - T_i} \quad (119)$$

The sensible energy and enthalpy of the mixture may then be expressed as:

$$\rho e_s = \sum_{k=1}^N \rho_k e_{s,k} = \rho \sum_{k=1}^N Y_k e_{s,k} \quad (120)$$

$$\rho h_s = \sum_{k=1}^N \rho_k h_{s,k} = \rho \sum_{k=1}^N Y_k h_{s,k} \quad (121)$$

A.2 The equation of state

The equation of state for an ideal gas mixture writes:

$$P = \rho r T \quad (122)$$

where r is the gas constant of the mixture dependent on time and space: $r = \frac{R}{W}$ where W is the mean molecular weight of the mixture:

$$\frac{1}{W} = \sum_{k=1}^N \frac{Y_k}{W_k} \quad (123)$$

The gas constant r and the heat capacities of the gas mixture depend on the local gas composition as:

$$r = \frac{R}{W} = \sum_{k=1}^N \frac{Y_k}{W_k} \mathcal{R} = \sum_{k=1}^N Y_k r_k \quad (124)$$

$$C_p = \sum_{k=1}^N Y_k C_{p,k} \quad (125)$$

$$C_v = \sum_{k=1}^N Y_k C_{v,k} \quad (126)$$

where $\mathcal{R} = 8.3143$ J/mol.K is the universal gas constant. The adiabatic exponent for the mixture is given by $\gamma = C_p/C_v$. Thus, the gas constant, the heat capacities and the adiabatic exponent are no longer constant. Indeed, they depend on the local gas composition as expressed by the local mass fractions $Y_k(x, t)$:

$$r = r(x, t), \quad C_p = C_p(x, t), \quad C_v = C_v(x, t), \quad \text{and} \quad \gamma = \gamma(x, t) \quad (127)$$

The temperature is deduced from the the sensible energy, using Eqs. 119 and 120. Finally boundary conditions make use of the speed of sound of the mixture c which is given by:

$$c^2 = \gamma r T \quad (128)$$

A.3 Conservation of Mass: Species diffusion flux

In multi-species flows the total mass conservation implies that:

$$\sum_{k=1}^N Y_k V_i^k = 0 \quad (129)$$

where V_i^k are the components in directions ($i=1,2,3$) of the diffusion velocity of species k . They are often expressed as a function of the species gradients using the Hirschfelder Curtis approximation:

$$X_k V_i^k = -D_k \frac{\partial X_k}{\partial x_i}, \quad (130)$$

where X_k is the molar fraction of species k : $X_k = Y_k W/W_k$. In terms of mass fraction, the approximation 130 may be expressed as:

$$Y_k V_i^k = -D_k \frac{W_k}{W} \frac{\partial X_k}{\partial x_i}, \quad (131)$$

Summing Eq. 131 over all k 's shows that the approximation 131 does not necessarily comply with equation 129 that expresses mass conservation. In order to achieve this, a correction diffusion velocity \vec{V}^c is added to the convection velocity to ensure global mass conservation (Poinsot and Veynante, 2001) as:

$$V_i^c = \sum_{k=1}^N D_k \frac{W_k}{W} \frac{\partial X_k}{\partial x_i}, \quad (132)$$

and computing the diffusive species flux for each species k as:

$$J_{i,k} = -\rho \left(D_k \frac{W_k}{W} \frac{\partial X_k}{\partial x_i} - Y_k V_i^c \right), \quad (133)$$

Here, D_k are the diffusion coefficients for each species k in the mixture (see section § A.6). Using Eq. 133 to determine the diffusive species flux implicitly verifies Eq. 129.

A.4 Viscous stress tensor

The stress tensor τ_{ij} is given by the following relations:

$$\tau_{ij} = 2\mu(S_{ij} - \frac{1}{3}\delta_{ij}S_{ll}), \quad (134)$$

and

$$S_{ij} = \frac{1}{2} \left(\frac{\partial u_j}{\partial x_i} + \frac{\partial u_i}{\partial x_j} \right), \quad (135)$$

Eq. 134 may also be written:

$$\begin{aligned} \tau_{xx} &= \frac{2\mu}{3} \left(2\frac{\partial u}{\partial x} - \frac{\partial v}{\partial y} - \frac{\partial w}{\partial z} \right), & \tau_{xy} &= \mu \left(\frac{\partial u}{\partial y} + \frac{\partial v}{\partial x} \right) \\ \tau_{yy} &= \frac{2\mu}{3} \left(2\frac{\partial v}{\partial y} - \frac{\partial u}{\partial x} - \frac{\partial w}{\partial z} \right), & \tau_{xz} &= \mu \left(\frac{\partial u}{\partial z} + \frac{\partial w}{\partial x} \right) \\ \tau_{zz} &= \frac{2\mu}{3} \left(2\frac{\partial z}{\partial w} - \frac{\partial u}{\partial x} - \frac{\partial v}{\partial y} \right), & \tau_{yz} &= \mu \left(\frac{\partial v}{\partial z} + \frac{\partial w}{\partial y} \right) \end{aligned} \quad (136)$$

where μ is the shear viscosity (see section § A.6).

A.5 Heat flux vector

For multi-species flows, an additional heat flux term appears in the diffusive heat flux. This term is due to heat transport by species diffusion. The total heat flux vector then writes:

$$q_i = \underbrace{-\lambda \frac{\partial T}{\partial x_i}}_{\text{Heat conduction}} - \rho \underbrace{\sum_{k=1}^N \left(D_k \frac{W_k}{W} \frac{\partial X_k}{\partial x_i} - Y_k V_i^c \right) h_{s,k}}_{\text{Heat flux through species diffusion}} = -\lambda \frac{\partial T}{\partial x_i} + \sum_{k=1}^N J_{i,k} h_{s,k}, \quad (137)$$

where λ is the heat conduction coefficient of the mixture (see section § A.6).

A.6 Transport coefficients

In CFD codes for multi-species flows the molecular viscosity μ is often assumed to be independent of the gas composition and close to that of air² so that the classical Sutherland

²This introduces errors that are less important than those related to the thermodynamic properties.

law can be used:

$$\mu = c_1 \frac{T^{3/2}}{T + c_2} \frac{T_{ref} + c_2}{T_{ref}^{3/2}} \quad (138)$$

where c_1 and c_2 must be determined so as to fit the real viscosity of the mixture. For air at $T_{ref} = 273$ K, $c_1 = 1.71\text{e-}5$ kg/m.s and $c_2 = 110.4$ K (White, 1999). A second law is sometimes preferred, called Power law:

$$\mu = c_1 \left(\frac{T}{T_{ref}} \right)^b \quad (139)$$

with b typically ranging between 0.5 and 1.0. For example $b = 0.76$ for air.

The heat conduction coefficient of the gas mixture can then be computed by introducing the molecular Prandtl number of the mixture as:

$$\lambda = \frac{\mu C_p}{P_r} \quad (140)$$

with P_r supposed as constant in time and space.

The computation of the species diffusion coefficients D_k is a specific issue. These coefficients should be expressed as a function of the binary coefficients D_{ij} obtained from kinetic theory (Hirschfelder et al., 1954). The mixture diffusion coefficient for species k , D_k , is computed as (Bird et al., 1960):

$$D_k = \frac{1 - Y_k}{\sum_{j \neq k}^N X_j / D_{jk}} \quad (141)$$

The D_{ij} are complex functions of collision integrals and thermodynamic variables. For a DNS code using complex chemistry, using Eq. 141 makes sense. However in most cases, DNS uses a simplified chemical scheme and modeling diffusivity in a precise way is not needed so that this approach is much less attractive. Therefore a simplified approximation is often used for D_k . The Schmidt numbers $S_{c,k}$ of the species are supposed to be constant so that the binary diffusion coefficient for each species is computed as:

$$D_k = \frac{\mu}{\rho S_{c,k}} \quad (142)$$

Note that the Schmidt number for each species k is assumed to be constant in time and space. P_r and $S_{c,k}$ model the laminar (thermal and molecular) diffusion. Usual values of Schmidt and Prandtl numbers for premixed flames are those given by PREMIX in the burnt gas.